INTEGRATING GROUND-PENETRATING RADAR, FIELD DATA, AND GEOGRAPHIC INFORMATION SYSTEMS FOR PALEOFLOOD STUDIES ALONG LYTLE CREEK, MURFREESBORO, TENNESSEE

By

Oluwatosin Isaac Obe

APPROVED:

Graduate Committee:

____

Chairman: Dr. Joe Collins

____

Dr. Henrique Momm

____

Dr. Jeremy Aber

____

Dr. Henrique Momm, Chairperson Department of Geosciences

____

Dr., Dean of the College of Graduate Studies

INTEGRATING GROUND-PENETRATING RADAR, FIELD DATA, AND GEOGRAPHIC INFORMATION SYSTEMS FOR PALEOFLOOD STUDIES ALONG LYTLE CREEK, MURFREESBORO, TENNESSEE.

By

Oluwatosin Isaac Obe

A thesis submitted in partial fulfillment

of the requirements for the degree of

MASTER OF SCIENCE

in

Geosciences

Middle Tennessee State University

April 2021

ACKNOWLEDGEMENTS

I give God Almighty the glory and praise for His help, protection, and mercies throughout my course of study in the program. My utmost gratitude goes to my parents for assisting me in achieving my goals in life. Without their contributions, I would not be able to come this far.

In a sincere appreciation, I want to thank my supervisor and advisor, Dr. Joe Collins, who has demonstrated a fatherly figure and shown inestimable concerns towards my carrier path. He stood by me despite all odds and trials being an international student.

My heartfelt appreciation goes to all the professors in the geosciences department. I want to thank especially Dr. Henrique, Dr. Racha, Dr. Aber, and Dr. Harris. I thank you so much for impacting my life positively. Thanks for your advice and encouragement.

I humbly thank all the GEOL 4020 geomorphology students for their contributions to my field survey. They made my data gathering a lot easier.

A special gratitude to Murfreesboro Recreations and Parks for allowing me to carry out research on the park. Also, I would like to appreciate Dr. Howard Cyr who constantly helped me to interpret my GPR data.

Finally, I want to thank all my friends who I have had the chance to meet in the class and the field in the likes of Andrew Osborne, Andrew Gibson, Miranda, Charlotte, Sarah, Kristie, Hannah, and others. Thank you all.

ABSTRACT

A geophysical investigation involving ground-penetrating radar (GPR) with soil probing was carried out on the floodplain of Lytle Creek, Murfreesboro, to understand the flood depositions and their subsurface lithology. Information was used to determine the watershed boundaries. A 350 MHz and 900 MHz Geophysical Survey Systems Inc. (GSSI) equipment was used for GPR data acquisition, and major interpretation procedures involving dewowing, filtering, and applying automatic gain were carried out. The GPR surveys in this study revealed significant sub-surface stratigraphy of depositional materials along the river channel. Three main characteristic radar facies were identified through the floodplain and bank exposure investigation. The majority of the profiles were noted to have horizontal, wavy, and hyperbolic reflections. The resulting floodplain structure was delineated and found to extend throughout the river channel and having fine-grained deposits (silty loam and silty clay). GPR proved to be a reliable tool in delineating subsurface stratigraphy non-invasively for this study.

TABLE OF CONTENTS

LIST OF TABLES

LIST OF FIGURES

LIST OF ABBREVIATIONS

DEM – Digital Elevation Model

GIS – Geographic information systems

GPR – Ground penetrating radar

GPS – Global Positioning Systems

GSSI – Geophysical Survey Systems Incorporation

LIDAR – Light Detection and Ranging

RADAR – Radio Detection and Ranging

SWD – Slackwater Deposits

USDA – United State Department of Agriculture

USGS – United State Geological Survey

CHAPTER I

INTRODUCTION

Due to atmospheric warming, flooding has become more hazardous (Wilhelm et al., 2018). Reducing uncertainties in reconstructing historical flood frequency and magnitude remains an important challenge. In Murfreesboro, Tennessee, extreme floods along the Stones River have been reported in 1902, 1948, and 1951 that caused damages to properties and lives (U.S. Army Corps of Engineers, 1966). Understanding floodplain development and evolution allow for more accurate predictions of future occurrences of floods and how to best mitigate the severity of these flood events.

Therefore, the purpose of this research was to characterize floodplain geomorphological structure and evolution along the lowest reach of Lytle Creek, ~ 700 m upstream from its confluence with Stones River, using ground-penetrating radar (GPR). This research had two main objectives: 1) to evaluate the feasibility of integrating geographic information systems (GIS) with GPR to describe and interpret the subsurface stratigraphy along Lytle Creek, and 2) to correlate exposed sedimentary profiles and their grain-size distributions to processed GPR profiles.

Previous Flooding in Murfreesboro, Tennessee

Flood events of high magnitude were recorded in 1902, 1944, 1945, 1948, 1955, 1963, and 1975. These events caused extensive damage to highways, railroads, homes, bridges, businesses, and public facilities. Each high magnitude flood event has an estimated peak discharge in excess of 20,000 cubic feet per second (cfs) (Bradley and Hileman, 2006). The flood event of March 28, 1902, was one of the highest events with an estimate peak discharge of

50,000 cfs. The flooding events that occurred on February 13, 1948 had a peak discharge of 38,000 cfs reaching me a flood stage of 22.73 feet (Bradley and Hileman, 2006). Law (2002), noted that the overflow of the West Fork Stones River into the natural floodplain was an infrequent event that contributed to the flooding. Additionally, sinkhole flooding constituted a hazard during the flooding event of March 1975 along Johnson Street (near Todd's Lake Sinkhole configuration) that resulted in the damaging of twelve homes at a water depth of ~ 7 feet (Federal Emergency Management Agency, 1999; FEMA). The USGS WaterWatch (2020) used the data collected from the gage station (USGS 03428200) at West Fork Stones River to determine the mean discharge, flood peaks, and highest discharges along West Fork Stones River (Figure 1).

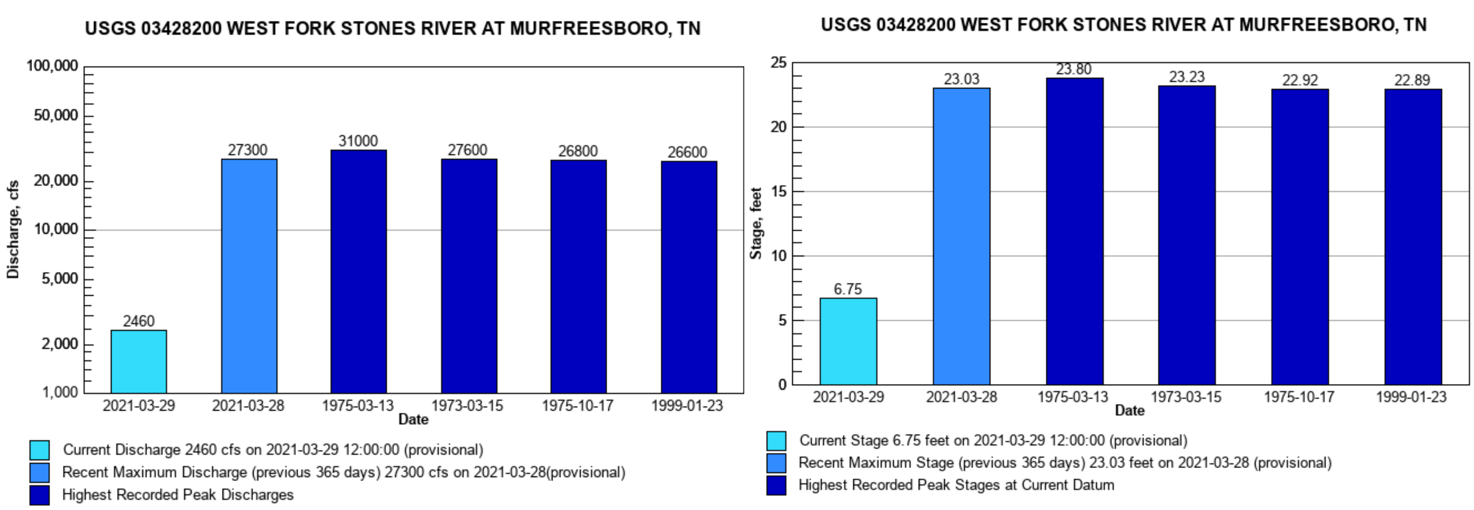

(a) (b)

Figure 1: Recorded values for (a) Discharge and (b) Stage (height) of the years having high magnitude of flooding events. (Modified after USGS WaterWatch 2020).

Lytle Creek Watershed

The Lytle Creek watershed has an approximate area of 26.14 sq. miles and lies within the Stones River watershed. The main river, Lytle Creek is a tributary of the West Fork Stones River and flows through the central commercial and industrial area of the City of Murfreesboro, Tennessee and drains an area of approximately 26.2 sq. miles (Figure 2). The width of the floodplain within the Lytle Creek watershed ranges from 100 feet to 700 feet wide, with the bank averaging 4 feet above the streambed (FEMA, 2008). The overall water quality of the watershed is controlled by tributaries to the channel. The watershed is surrounded by springs such as Spring Branch, Black Fox Spring, and Murfree Spring that have been monitored extensively as a potential source of pollution to Lytle Creek (Murfreesboro Stormwater Program, 2013; MSP). The land use within the watershed is a blend of agricultural, commercial, residential, and industrial activities (Figure 3). A 1 m spatial resolution digital elevation model (DEM) generated from Light Detection and Ranging (LIDAR) technology was used to characterize topography and subsequently determine channel network (Figure 4). The Lytle Creek flows roughly northeastward to the Stones River. Understanding the concept of stream-channel cross-sectional area is an important component in determining any direct estimate of discharge at flood stage. Similarly, calculating the longitudinal profiles can help define the active zone of bedload transport (Spicer and Costa, 1997).

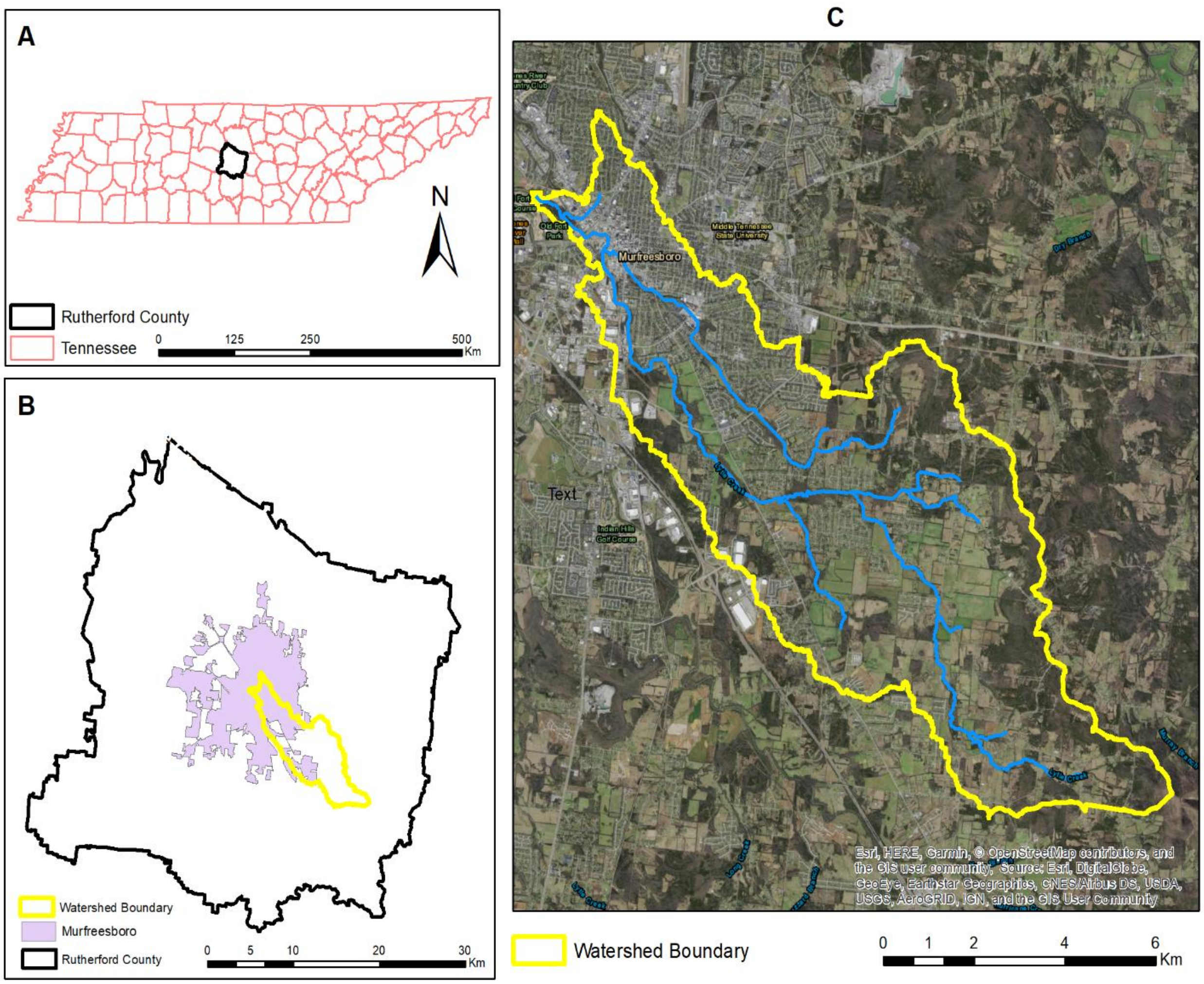

Figure 2. Lytle Creek is located in Rutherford County, Tennessee (a) It drains through the city of Murfreesboro (b) being composed of rural and urban land covers, and (c) the entire Lytle Creek watershed with the Channel Network.

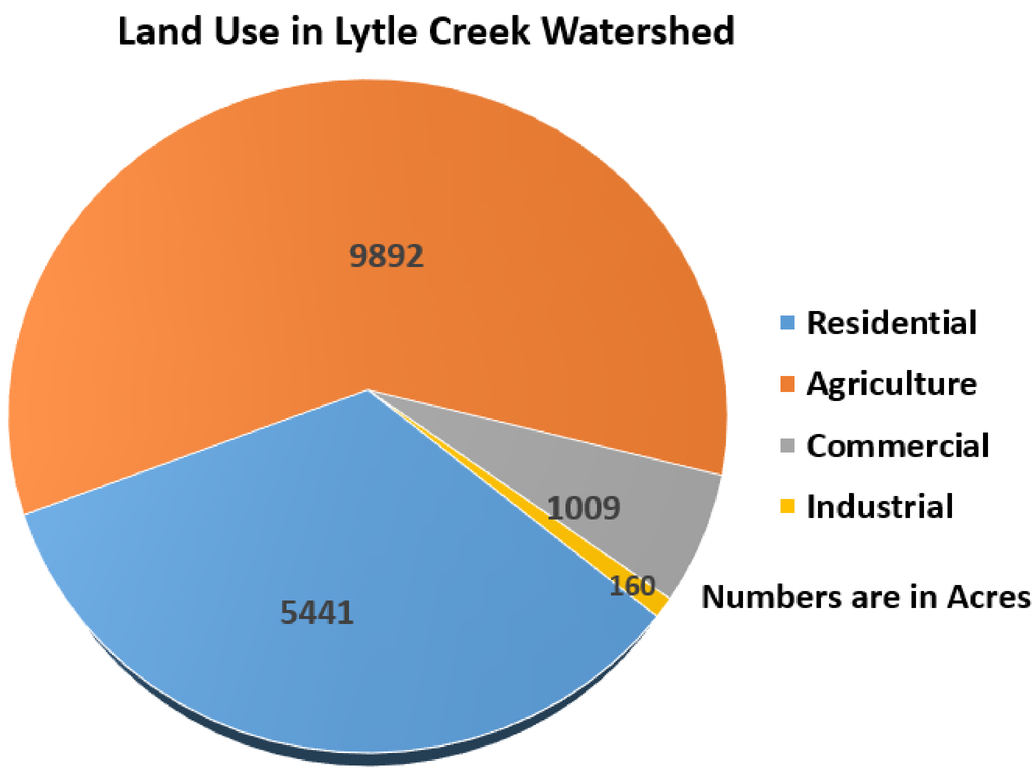

Figure 3: Landuse in Lytle Creek Watershed (modified after MSP, 2013).

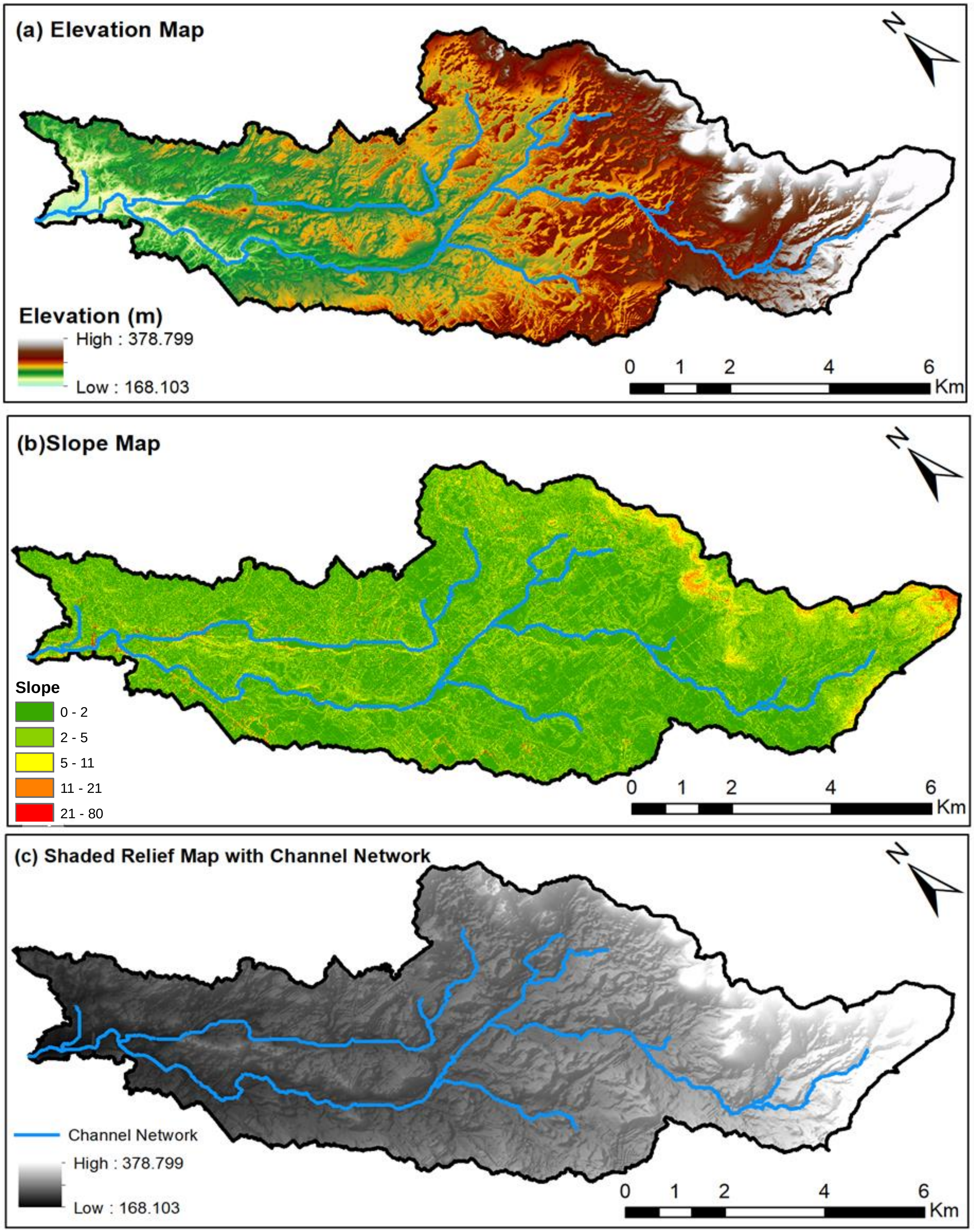

Figure 4. Description of (a) elevation, (b) slope, and (c) shaded relief for Lytle Creek.

Floodplain Development

Floodplain construction can be explained both hydraulically and genetically. The hydraulic floodplains are constructed at surfaces adjacent to the channel and mainly noticeable at the active boundaries channels which produces a stable conduit for the transportation of water and sediments (Nanson and Croke, 1992). The genetic floodplains can be defined as the largely horizontally-bedded alluvial landform, separated from the channel by banks, and made of sediments moved by the present flow-regime (Nanson and Croke, 1992). Hydrology plays an important role in the formation and evolution of floodplains. Floodplains along West Fork Stones Rivers can be described in three classes comprising: 1) high-energy, non-cohesive, 2) medium-energy non-cohesive, and 3) low-energy cohesive (Nanson and Croke, 1992). The non-cohesive comprising the high and medium energy are disequilibrium and dynamic landforms which erodes, either completely or partially, due to infrequent flood events (Nanson and Croke, 1992). Examples of these floodplains are found in steep confining bedrock valleys which transport very coarse sediments. The sorting is poor (gravel and sands) and forms lateral and vertical accretion. The low-energy cohesive is formed predominantly due to overbank depositions involving a high proportion of suspended-load materials (sand and silt) (Figure 5).

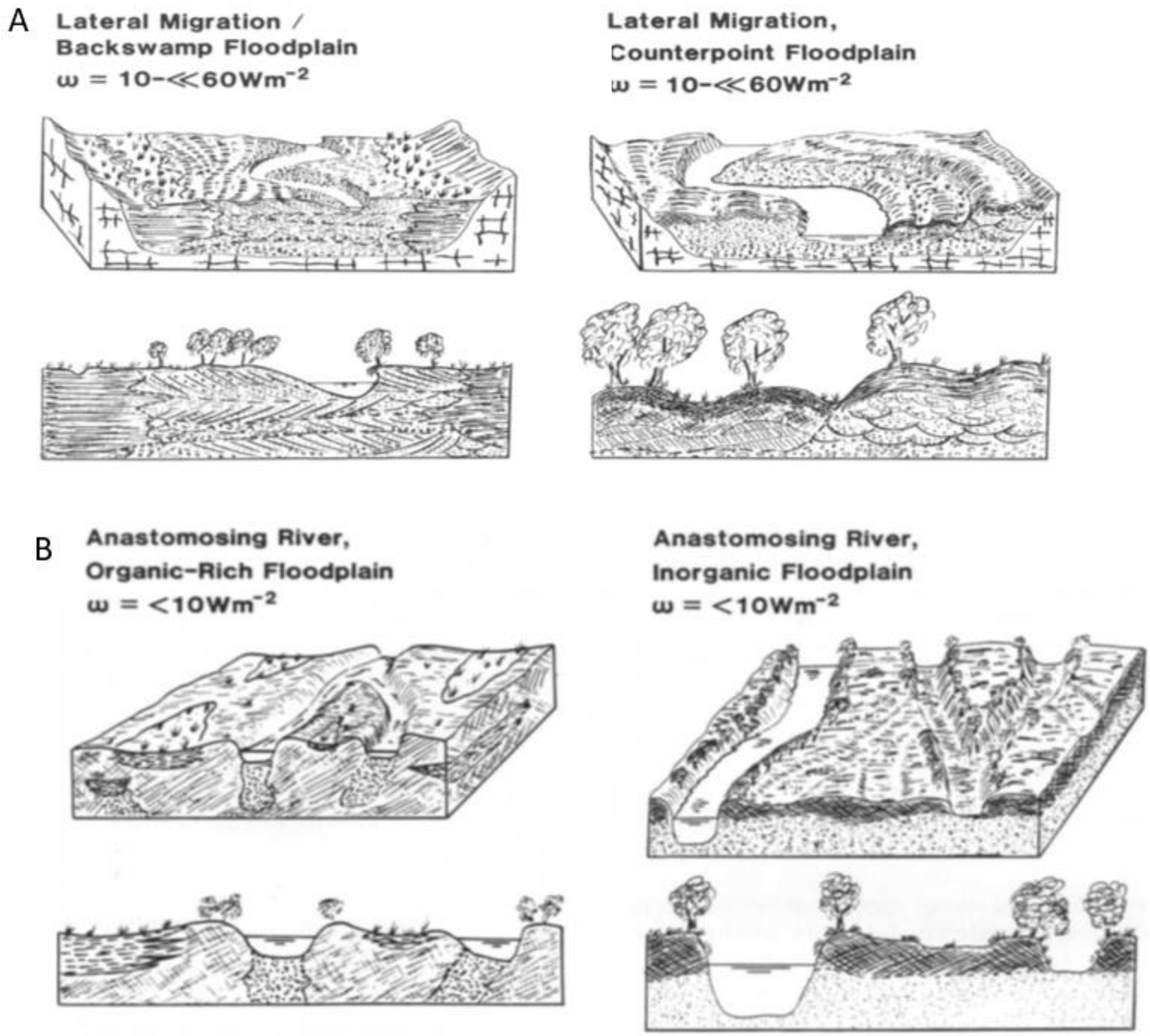

Figure 5: (a) Lateral migration/backswamp floodplain and lateral counterpoint floodplain (Examples of high and medium energy-level) and (b) Anastomosing river, organic-rich floodplains and inorganic floodplains (Low-energy) (Nanson and Crook, 1992).

These classes govern the range of floodplain studies and how their formations influence the geomorphology of river channels. The formation and evolution of floodplains are often described by the concepts of stream power (the stream's ability to do work), and shear stress (ability to entrain and transport sediment). Channel floodplain is essential to understanding the amount and texture of the sediment loads (Schumm and Khan, 1972). Anthropogenic activities, mass-movement, and aeolian processes also contribute to floodplain formation in a particular environment (Nanson and Croke, 1992).

Geomorphologists have suggested that the physical processes involved in the formation of a floodplain are enormous, and diverse in their types. These suggestions require the development of a procedure to describe the type and class of the floodplain within a region (Dott and Bourgeois, 1983). Some floodplain depositional processes can either be laterally (juxtaposed point-bar deposits) or vertically (single-thread channels) accreted (Allen, 1965). However, Jackson (1978), suggested that lateral accretion is not necessarily the main factor of floodplain formation and point bars are not always a primary sedimentary landform. The main geomorphic features of the floodplain formation, which are notable for this research, are lateral point-bar and overbank vertical-accretion (Nanson and Croke, 1992). The progressive depositions of point bars cause lateral point-bar accretion to occur along the river channel, creating a new floodplain with disjointed deposits. Examples are aggregates of gravels and sand deposits. The dominant vertical accretion results from the overbank depositions of flood sediments (Figure 6).

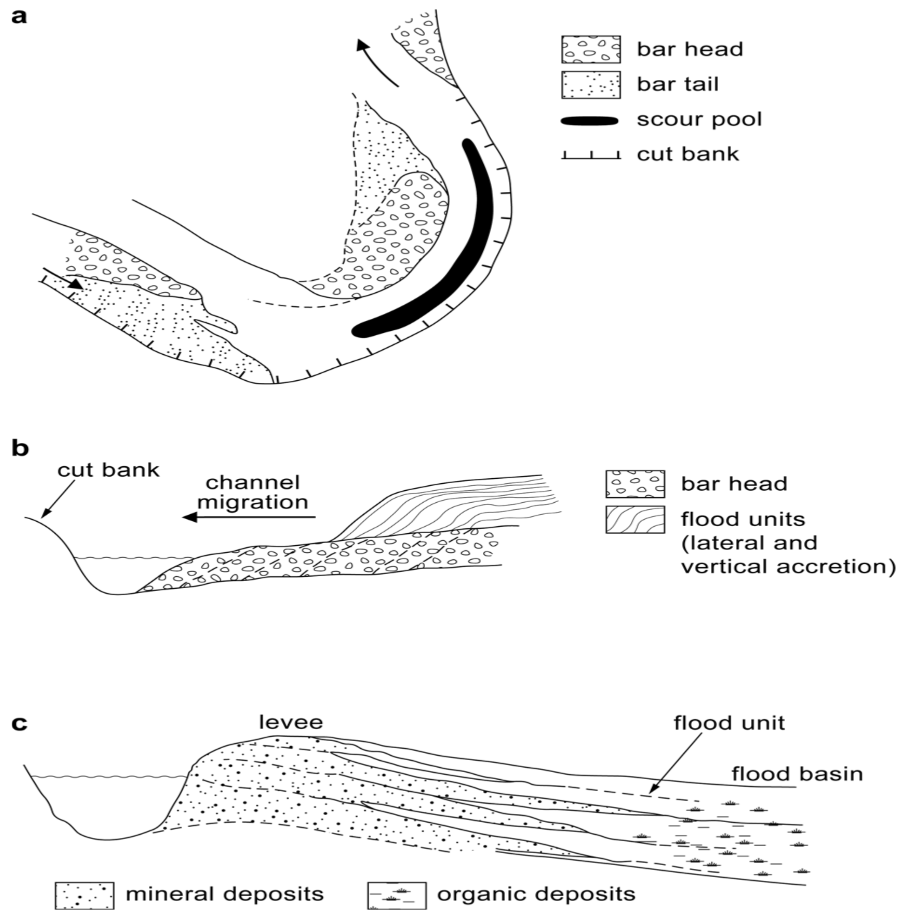

Figure 6. Flood sediment units, showing (a) in-channel bedforms, (b) channel margin accretion and (c) floodplain depositional sites (Jones et al., 2010).

Understanding the development of floodplains within watershed can lead to an estimation of past flood (paleoflood) frequencies and supporting the generation of knowledge of past flood events not available in traditional records (Ely et al., 1992; Kochel and Baker, 1982; Costa, 1978). The emergence of paleoflood hydrology took place in the 1970s and 1980s, with research on paleoflood studies increasing in the 21st century. The term paleoflood hydrology resulted from the studies of flood frequency in numerous environments (Baker, 2008). Paleofloods are flood events that leave behind traces that are naturally observed (Baker, 2008). Evidence of past flooding can include features such as slackwater deposits, high watermarks and boulder bars, in addition to the floodplain itself. However, paleoflood hydrology has limitations due to localization of the results.

General Theory of GPR

Ground-penetrating radar (GPR) is a non-invasive geophysical method that images the subsurface by sending short pulses of electromagnetic energy (radio waves) using a transmitting antenna and measuring the differences in electromagnetic properties of subsurface features through the receiving antenna (Olhoeft, 1999; Harari, 1996). The interpretation of GPR is similar to that of seismic reflection, a traditional technique used in exploration geophysics, which involves the passage of electromagnetic energy into the subsurface and detecting the resulting signals. GPR uses a transmitting (Tx) and receiving antenna (Rx) in bistatic or monostatic mode (Figure 5). In bistatic mode, the Tx and Rx antennas are held apart in constant distance. In most cases, they are at zero-offset, which implies that the transmission point is the same as the receiving point. In monostatic mode, the Tx and Rx antennas are independent and can be used in different arrays in gathering information as shown in Figure 7 (Tischler et al., 2002).

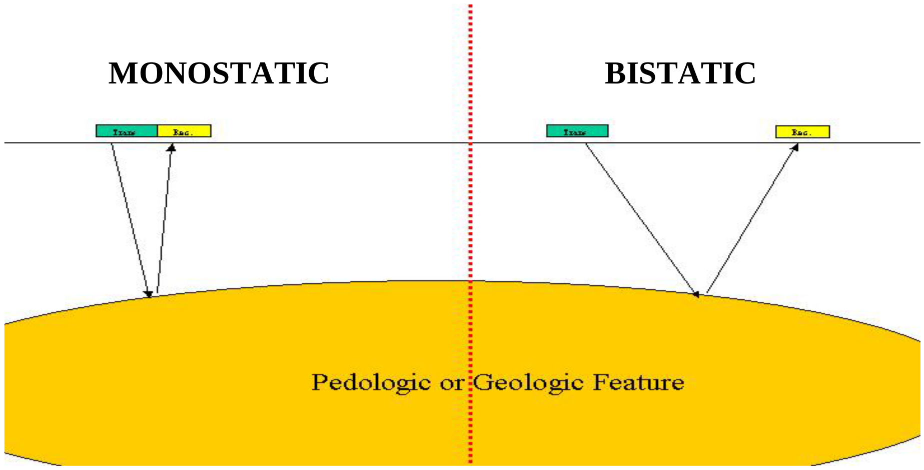

Figure 7: A monostatic and bistatic antenna configuration. (Green (Tx) and yellow (Rx) (Tischler et al., 2002).

The choice of antenna depends on the desired output (depth of penetration and resolution of interest) and soil condition. The deepest depth at which a GPR signal travels and the ability to differentiate features of different sizes can be defined as the depth of penetration and resolution respectively. The higher the frequency of the antenna, the lesser the depth of penetration, and vice versa (Figure 8) (Radzevicius et al., 2000). The goal of a project determines the frequency that can be used.

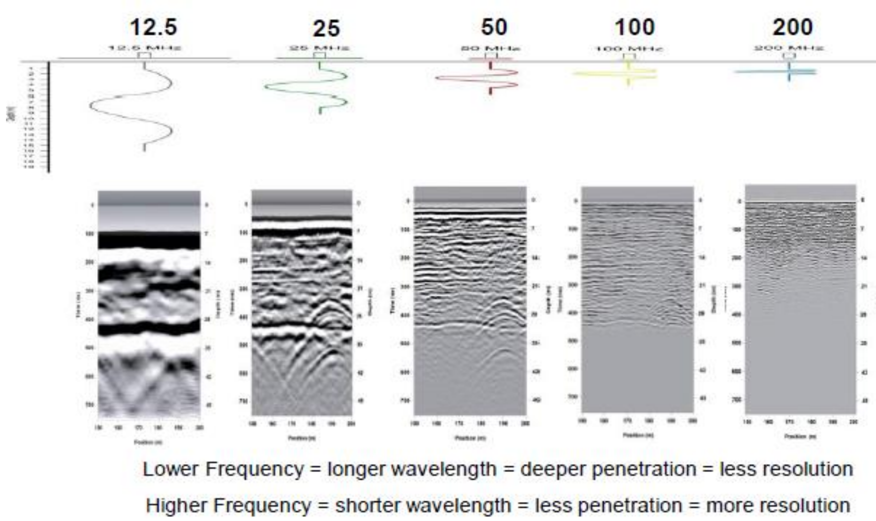

Figure 8: Antenna frequency with relative depth of penetration and resolutions (Modified after Sensor and Software, 2017).

The propagation of a pulse is dependent on dielectric permittivity (dielectric constant). A dielectric constant is a measure of the ability of a material to retain charges when an electric field is introduced. The dielectric properties of materials influence how electromagnetic energy can be transmitted into the subsurface (Table 1). According to Utsi (2006) a measurable radar reflection requires a significant electromagnetic contrast between two interfaces. Loss of radar energy (attenuation) is a complex function of the electric and dielectric properties of a media through which a radar signal travels. Conductivity, relative magnetic permeability, and dielectric permittivity control the attenuation factors in a material. The dielectric contrast occurs when the radar encounters a sharpness in the subsurface material and the resulting wave tends to record the interface between the materials, and help to distinguish between different sedimentary layers in the subsurface (Figure 9).

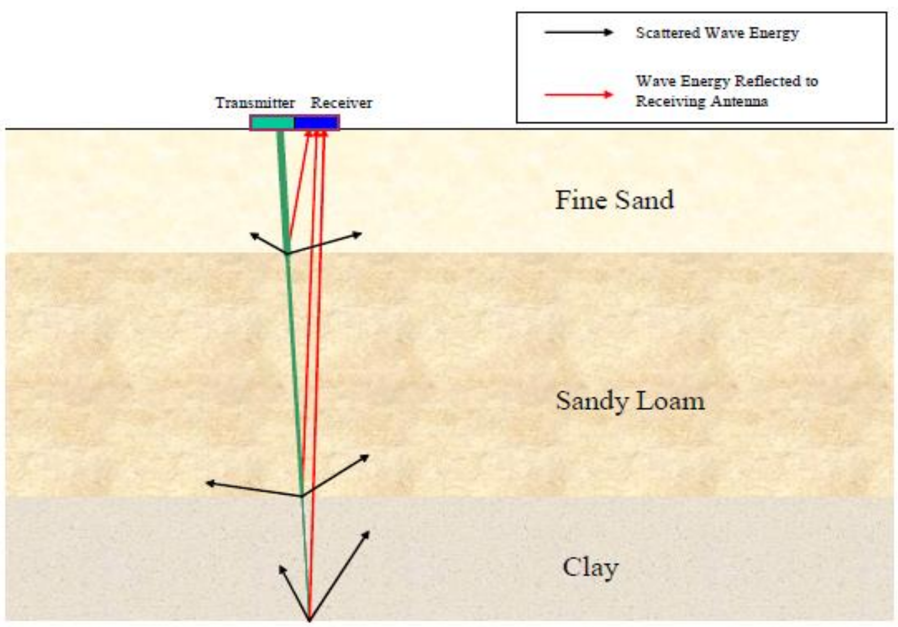

Figure 9: GPR wave propagation, scattering and reflection. *(As a GPR electromagnetic waves encounters different horizons, the wave is scatters partially, some are reflected back to the receiving antenna and other backscattered energy are lost due to the dielectric constant)* (Tischler et al., 2002).

Table 1. Dielectric constants of different materials. (Modified after Tischler et al., 2002).

Material	**Dielectric Constant**	**Material**	**Dielectric Constant**
Air	1.0	Wet Sandstone	6.0
0Snow	1.5	Wet Granite	6.5
Dry Loamy/Clayey soil	2.5	Travertine	8.0
Dry clay	4.0	Wet limestone	8.0
Dry sands	4.0	Wet Basalt	8.5
Ice	4.0	Tills	11.0
Coal	4.5	Wet Concrete	12.5
Asphalt	5.0	Volcanic ash	130
Dry Granite	5.0	Wet sands	15.0
Frozen Sand &Gravel	5.0	Wet Sandy Soils	23.5
Dry Concrete	5.5	Dry Bauxite	05.0
Dry Limestone	5.5	Saturated Sands	25.0
Dry Sand & Gravel	5.5	Wet Clays	27.0
Potash Ore	5.5	Peats	61.5
Dry Mineral/Sandy Soil	6.0	Organic Soils	64.0
Frozen Soil or Permafrost	6.0	Sea water/Water	81.0

.

There are different methods of collecting GPR data, but the most common method is the common offset (Figure 10) which was primarily used for this research. This method requires a single transmitting and receiving antenna. It is expedient that major research regarding paleoflood studies use common-offset, 2-D radar reflections to explain the subsurface lithology (Bridge et al., 1995).

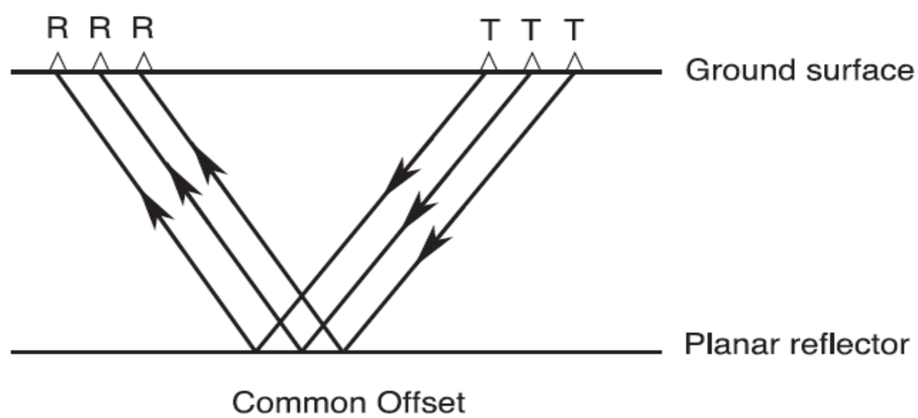

Figure 10: The geophysical reflection survey used for the study area (Modified after Neal, 2003). *Note: T = transmitter, and R = receiver.*

GPR has been successfully used in a wide range of applications. In archeological and historical studies, it has been used to investigate shallow graves, headstones, old pathways, buried items, and hidden foundations (Riley and Johnson, 2004). Kowalsky et al. (2004) used GPR to determine the depth of the groundwater table, contamination zones, groundwater flow, and groundwater salt content (Tsofilias and Becker, 2008). The GPR method also has advanced road and pavement studies in determining pavement layer thickness, cavity, voids, and rutting (Ronen et al., 2018; Evans, 2009; and Wright, 2019). GPR can be used in geologic and environmental studies to understand the depth-to-bedrock of groundwater, sand dunes and glaciers studies, identification of wash-over deposits, flood plain and deposition studies, and identification of fracture and faults (Adetunji et al., 2008; Bakker, et al., 2006; Jones et al., 2007).

Ground-penetrating Radar (GPR) applied to Floodplain Study

There has been a steady increase in scientific publications of GPR and GIS for sedimentology and paleoflood studies since 1976 (Figure 11).

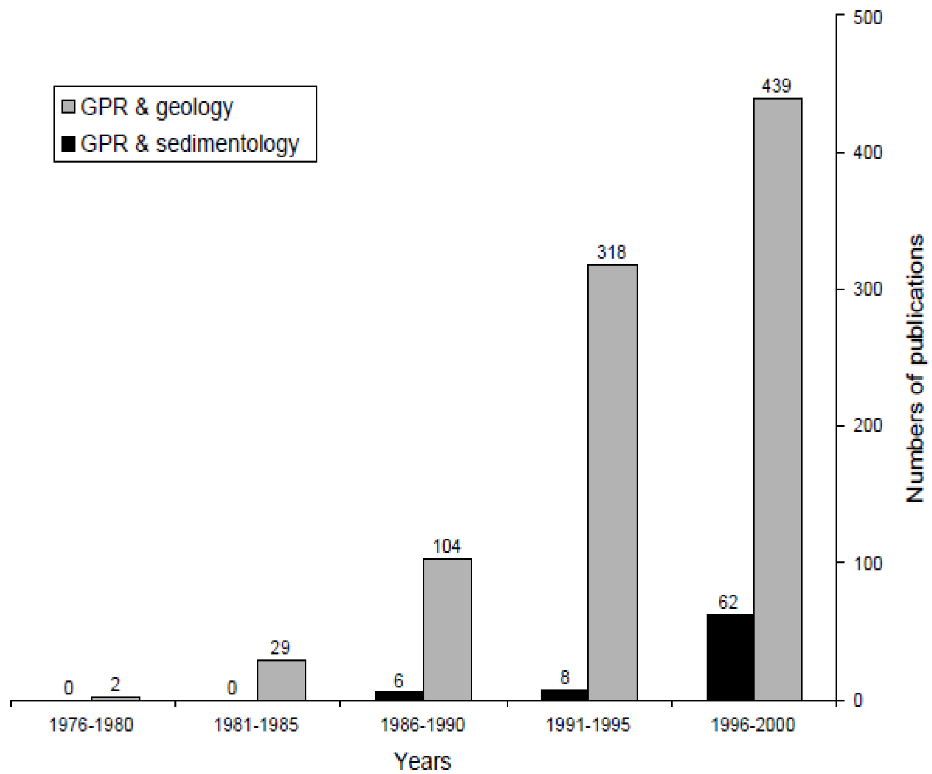

Figure 11: Development of GPR to sedimentology to paleoflood studies (Modified after Harari, 1996).

GPR is primarily used for the study of subsurface features such as stratigraphic architecture, sand-body geometry, and for correlating sedimentary layers. It was first introduced in the late 1960s by the US military for subsurface tunnel investigations (Bristow and Jol, 2003). GPR has since been used for imaging and characterizing fluvial sediment facies and their geometry in 2-D and 3-D (Beres and Haeni, 1991). For example, Woodward et al., (2003), used GPR to explain differences in the sand-bed braided river in southern Saskatchewan, Canada. GPR also has been used in hydrological studies to image fluvial sediments in order to provide information on fluvial stratigraphy and sediment compositions (Bristol and Jol, 2003). Ekes and Friel, 2003, used GPR combined with geochronological data to explain the evolution of an alluvial fan sequence. Okazaki et al., 2015, used GPR for hazard assessment and the formation of an alluvial fan of gravelly braid bars in the Abe River, central Japan, and to explain three-dimensional variations. GPR has also been used in sedimentological studies to reconstruct past depositional environments and help to improve groundwater investigation. (Neal, 2004).

Despite the importance of GPR to the study of subsurface lithology, few studies have been carried out to examine its applicability to paleoflooding studies because of the high attenuation of nearby water bodies. The assumption is that GPR is not a viable technique in highly-moist environments due to high conductivity of water (Jones et al., 2007). Nevertheless, Spicer et al. (1997) carried out an investigation using GPR to measure stream-channel cross-sections at high flow rates. The GPR equipment was suspended from a bridge and data was collected along the stream channels. The 100 MHz antenna showed a reasonable depth of penetration and resolution. Stream-flow data was correlated with the radar signal velocity to validate the GPR profile. The probable GPR test proved to be 20% accurate in determining the stream-channel profile. Leopold et al., (2006) carried out an investigation using GPR in classifying the sedimentary characteristics of fluvial deposits in the Namib Desert. The classification allowed a better understanding of fluvial regimes, which are influenced by river-bed morphology, sediment size, and water energy. A combination of GPR and geomorphological-sedimentological analysis with dating control by optical stimulated luminescence (OSL), provided a validity to the approach in the study. The floodplains along River Waal in the Netherlands were profiled using the GPR radar facies and borehole sedimentary facies to determine radar velocity. Their results show that overbank mud drapes and sand deposition occurred along the river channel during flood events. Overbank sands were noted at the top layer and the deeper coarse-grained channel deposits could be imaged using GPR but were retrieved using core samples (Bakker et al., 2007). According to Baker et al., (2007), the development of sand bars were more widespread in embanked flood plains. The sand bars were deposited during the recent flooding. The GPR profile showed the deposition comes due to progressive land reclamation and acted as a sediment enclosure for silty clay, clay, and fine sand. Also, the core samples showed the layers in which the sediments were deposited.

In this study, the GPR method provides a rapid means of acquiring subsurface data from river channels, terraces and floodplains and interpretation of the radar profiles in combination with the radar facies and stratigraphy, and bank exposure analyses will provide evidence to corroborate the GPR data.

Regional Setting of Murfreesboro

Murfreesboro, Tennessee, is located within the Central Basin of Tennessee and is characterized by rolling hills and valleys covered by pasture, glade, and forest (Law, 2002). Flat-lying limestone beds are common in the area, with land elevations ranging between 500 and 600 feet above sea level, and characterized by a karst topography (Bradley and Hileman, 2006) (Figure 12). The region experiences moderate winters and warm, humid summers with temperature ranging between 0^{0}F and 100^{0}F in most cases. The average annual rainfall is approximately 53.5 inches (Law, 2002). Large frontal storms occasionally lead to flooding in the area during the winter months (December through March), and high-intensity thunderstorms mostly result in flooding during the spring and summer months (April through September) (Law, 2002).

According to the 1977 U.S. Department of Agriculture (USDA) soil survey of Rutherford County, the soils are mainly composed of the Lynnville series, which is a deep, moderately well-drained soil, originating from the limestone bedrock. Lynnville silt loam is a major component in this series characterized by a moderately well-drained loamy silty soil and mottled clay that can be observed within 1 to 3 feet of the weathered limestone. The water table is high which allows the soil to be saturated in the winter and spring (USDA, 1977).

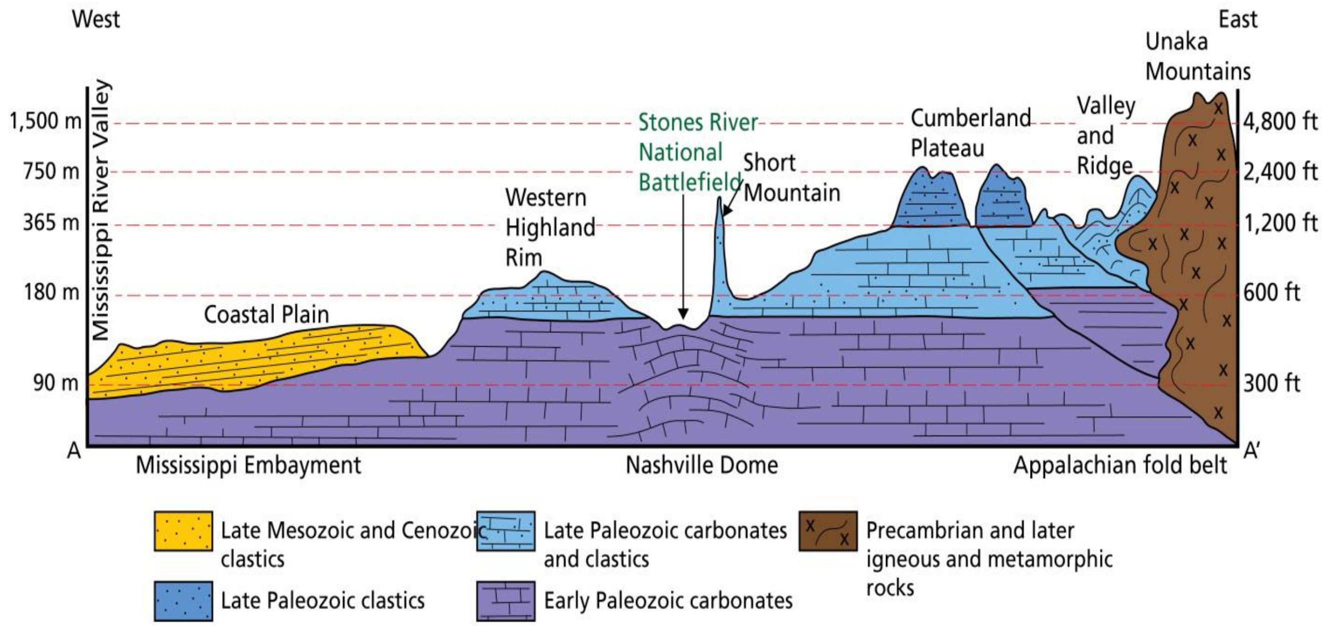

Figure 12: Schematic cross-sectional view through Tennessee. *The image shows the inverted topography of the Central Basin (Nashville Dome)* (Thornberry-Enrich, 2012).

The primary bedrock formations underlying the area are Ordovician-aged Lebanon, Pierce Murfreesboro, and Ridley Limestone (Law, 2002). The Lebanon Limestone is composed of 75-100 ft. of cryptocrystalline to very fine-grained, medium light-gray to brownish-gray and yellowish-brown limestone. The Ridley Limestone is composed of 100-150 ft. of cryptocrystalline to very fine-grained, brownish-gray and yellowish-brown limestone. The individual beds can be composed of coarse-grained sediment, and ranging from medium to thick units. The Pierce Limestone comprising cryptocrystalline to very fine-grained, brownish-gray and yellowish-brown limestone has a depth range of 25 ft. (Figure 13).

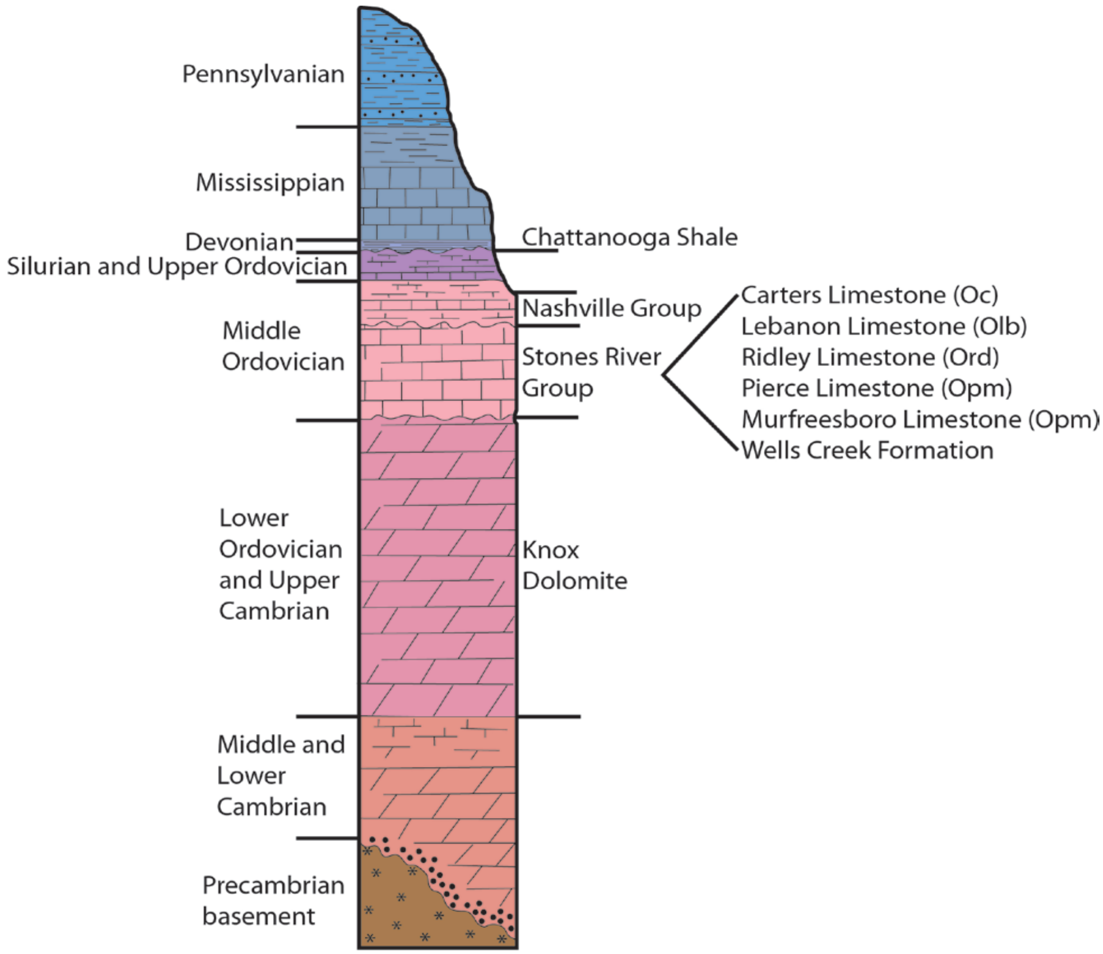

Figure 13: Stratigraphic column of the Nashville Dome in Central Tennessee. (*It shows the Ordovician formation comprising the Ridley, Pierce, Murfreesboro, and Lebanon Limestones which are typical of the study area*) (Thornberry-Enrich, 2012).

The formation of karst landscape along the Stones River poses hazards which include cave openings and collapses, sinkhole flooding, and sinkhole formation (Thornberry-Enrich, 2012). According to Thornberry-Enrich (2009), the natural fluvial processes in the West Fork Stones River causes the river to migrate and meander. The karst areas are vulnerable which can lead to flooding and transportation of contaminants. The three main mechanisms that contribute to the lowland flooding in the study area are direct storm input, increase in the groundwater level, and overflow from the West Fork Stones River.

CHAPTER II

MATERIALS AND METHODS

GPR Data Collection

The GPR unit used in this study was rented from the Department of Geosciences at the University of Tennessee, Knoxville, and manufactured by GSSI. The utility scan equipment features a wireless and lightweight configuration using HyperStacking technology with a maximum depth range of 10m (35 ft.). The system comprises 350 MHz and 900 MHz antenna for both distance and time-triggered sampling. It also includes a digital screen, four Lithium-ion batteries, rugged cables, and Trimble GPS. The 350 MHz antenna was selected as a compromise between the resolution and desired depth of penetration and the 900 MHz antenna was used for areas not accessible with lower frequency antenna (Figure 14).

Figure 14: A GSSI GPR instrument having a 350 MHz antenna.

GPR investigations were carried out between October 5 and October 9, 2020, along a 3.1mile stretch of riverbank and floodplain located along the lowest reach of Lytle Creek, just before its confluence with the West Fork of the Stones River (Figure 15). The GPR survey was aimed at determining reflection patterns in order to characterize stratigraphy within the floodplain. The survey was carried out in five locations, selected based on the proximity to the river channel and on the floodplain. Most of the places have been adjusted due to human activities which were used for recreational and commercial purposes. For example, dams have been constructed just upstream from the study area which affects the flow of water, and hence affects the flood depositions. Also, along the floodplain there is a city greenway along the banks of Lytle Creek. Nevertheless, the survey was selected based on places indicated to have been flooded and potentials for floodplain stratigraphy interpretation. A total of seven grid sections within the survey area with a maximum of 12 transects in each of the grids. The direction of the grids are in northeast to southwest and east to west direction. Common offset with a 2 m spacing was used in the entire grid. The dielectric constant was adjusted between 9 (wet soil) and 24 (dry soil).

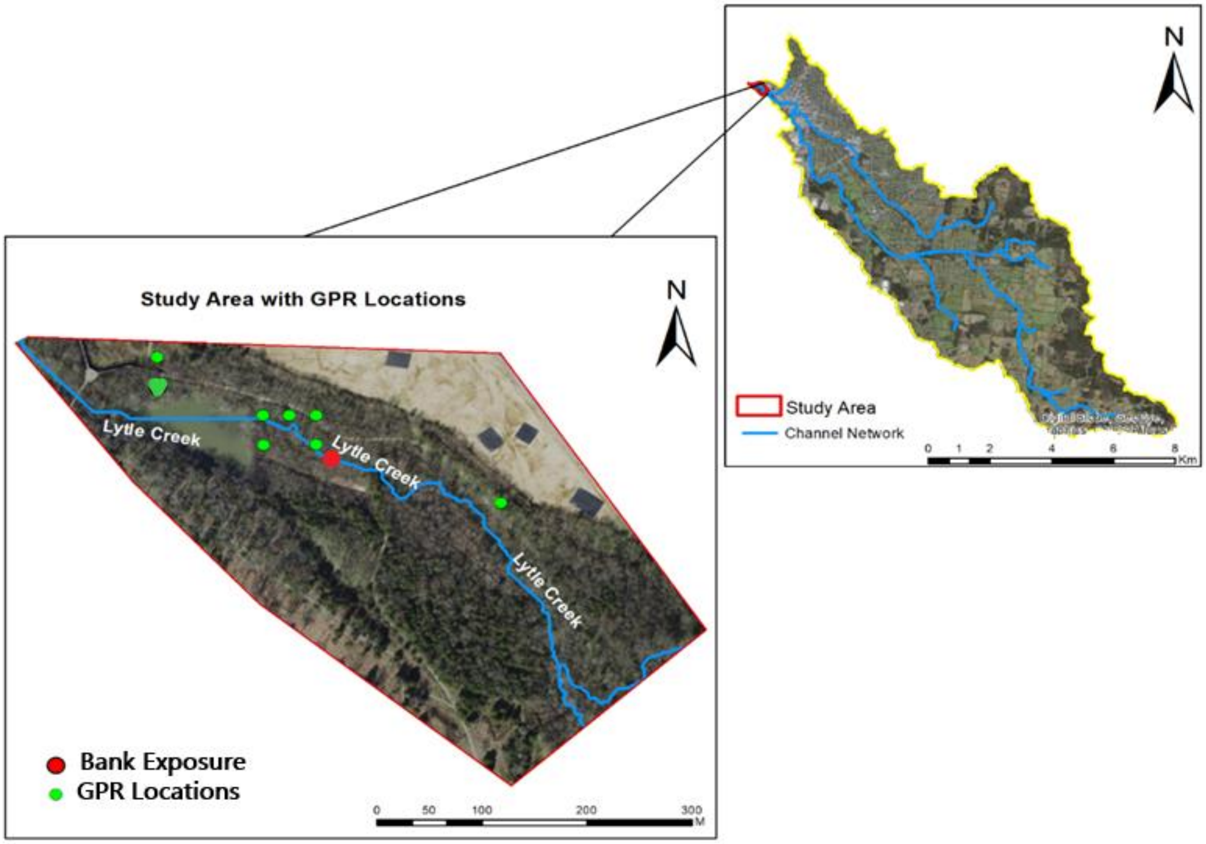

Figure 15: The study area showing the locations of GPR data collections.

Processing of the GPR data involved standard procedures, including background removal, low-frequency noise removal, static correction, trace-to-trace averaging to eliminate the horizontal disturbances as a result of the pavement and uneven surface, surface normalization, automatic gain control (AGC) (up to 12 ns), and data migration (Okazaki et al., 2015). All of t these procedures were carried out using the RADAN 7 software.

GPR data interpretation was based on radar stratigraphy from literature reviews. This procedure involves identification of reflections boundaries (Hugenholtz et al., 2007). Typical radar facies consist of a different set of reflections dependent on the shape, bedding and internal structure of the sediments, and their dip (Pellicer and Gibson, 2011) (Figure 16).

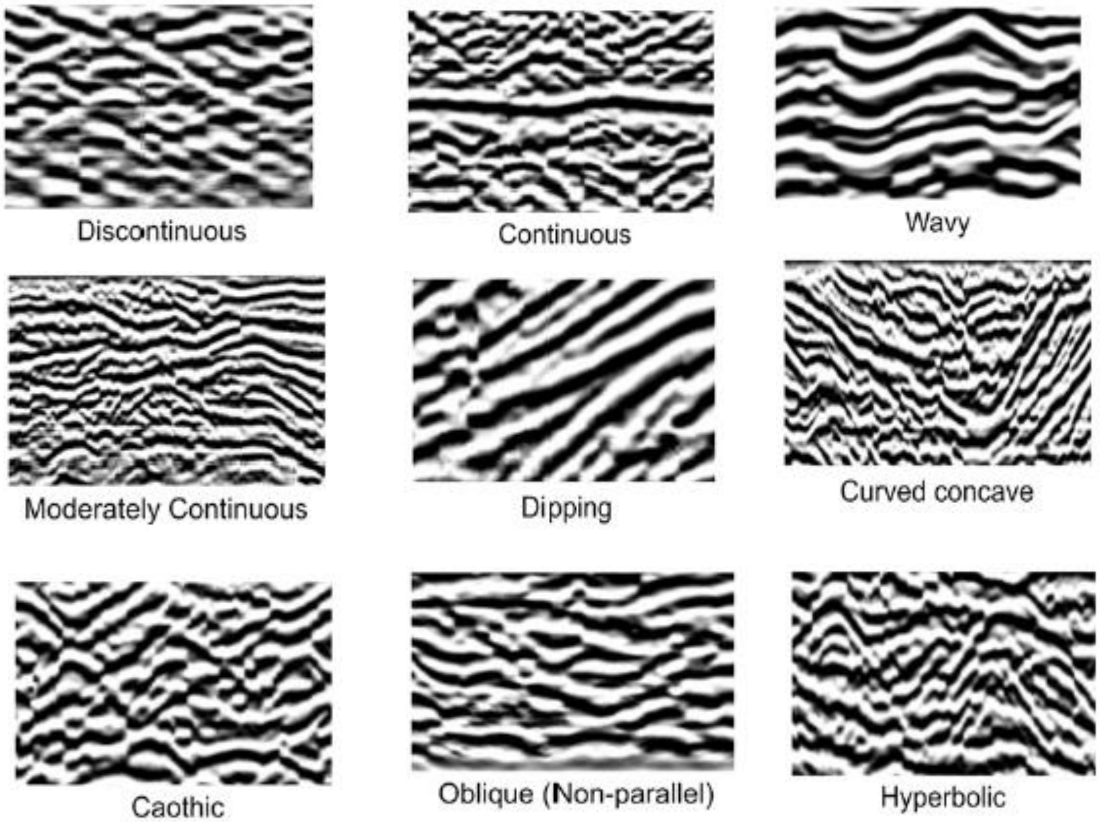

Figure 16: Common terminologies used in describing radar signatures. (Modified after Pellicer and Gibson, 2011).

Bank Exposure along River Channel

Soil samples are important for interpreting GPR survey data accurately (Baker, 2007). Stratigraphic descriptions of the soils within the study area were assayed from one bank exposure along Lytle Creek in conjunction with 350 MHz GPR scan in order to correlate grain size with GPR reflections (Stephanie, 2007). These descriptions were aimed at describing the lateral view by scrapping the surface and inspecting the differences in the lithology of the floodplain deposition by using a spade to clean out the weeded surfaces. The inspected location is perpendicular to the flow of the river channel (Figure 17). Three main sections (A, D, and F) were identified based on the visual analysis of the profile, the upper, middle, and the lower section, located at the middle of the river channel. The measurement for the stratigraphic profile was taken in centimeters below the ground surface. In describing the stratigraphic units, letters were assigned to each notable lithology unit. The stratigraphic units were described by (1) identifying the sediment colors using the Earth Colors chart; (2) nothing different changes in grain size; and (3) defining the different boundaries and sedimentary structures.

Figure 17: Bank Exposure along the river channel indicating floodplain structures.

A depth of 1.5 m was attained and the top 1 cm was noted to be layers where human activities have influenced. The base of the embankment profile is on bedrock. The grain size distributions of the sediment samples were then measured on a MALVERN Mastersizer 3000 outfitted with a HydroEV pump accessory.

Grain-size analysis

A total of 13 sediments samples, at 20 cm intervals were collected from the exposed bank for grain-size analysis. All the samples were processes for grain-size analysis following outlined by Collins et al., (2018) in which the samples were preheated with 0.5 ml 40% Hydrogen Peroxide (H_2O_2) to remove organics and then centrifuge to separate the organics from the sample. The samples were then deflocculated using 5 ml of sodium hexanetaphosphate (HMP $C_9H_{10}O_4$) prior to analysis. Results were then processed using the Mastersizer software program (Figure 18).

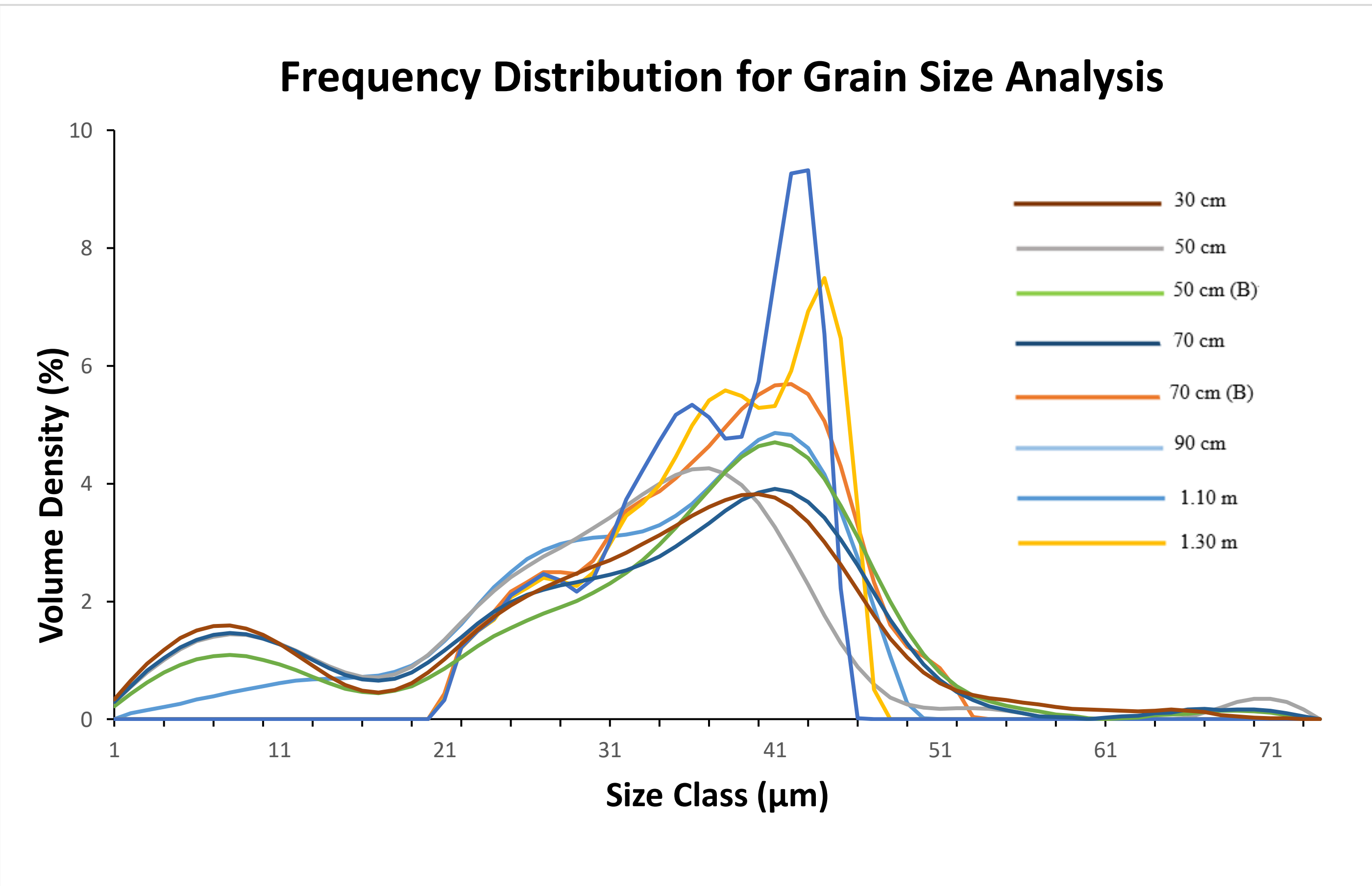

Figure 18: Frequency Distribution for the Grain Size analyses along Lytle Creek.

CHAPTER III

RESULTS AND INTERPRETATION

Bank Exposure Analysis

The upper sections of the soil profile and samples, at the center of the study area BE 1 (Figure 19), consisted of fine grained, fairly sorted, fining downward sequence of dark gray silty loam soil, and having silty clay with layers of dark brown to dark red silty loam reaching the bedrock. The description of the soil stratigraphy is shown in Table 3. The sedimentary profile rests on Ridley Limestone. In soil strata (A), the organic and weathered fragments were noticeable between 10 to 30 cm consisting of silty loam ranging in color from black to dark brown. The underlying layer (B) extends from 40 – 60 cm and is predominantly silty loam with a blend of silty clay loam as derived from the organic matter, with color ranging from strong brown to reddish yellow. The preceding layers C and D are similar in color but differ in soil texture as the upper portion has a silty clay loam texture and the lower portion has a continuation of silty loam soil. The soil ranges from 70 – 90 cm with coloration from strong brown to reddish yellow. The lowest layers E and F with depth between 1.0 – 1.3 m consists of silty loam and a bit of peat and clay that interface with rising water when it floods. Details of the sieve graphs can be seen in appendix A.

Table 2. Soil investigation along the river bank

Depth	Color Code	Color	Soil Texture
10.0 cm	10 YR 2/1	Black	Silty loam
20.0 cm	7.5 YR 3/1	Very Dark Gray	Silty Loam
30.0 cm	10 YR 3/3	Dark Brown	Silty Loam
40.0 cm	10 YR 4/2	Dark Gray Brown	Silty Clay Loam
50.0 cm	7.5 YR 3/4	Dark Brown	Silty Clay Loam
60.0 cm	7.5 YR 4/6	Strong Brown	Silty Loam
70.0 cm	7.5 YR 5/8	Strong Brown	Silty Loam with Sand
80.0 cm	5 YR 7/8	Reddish Yellow	Silty Loam with Sand
90.0 cm	7.5 YR 6/6	Reddish Yellow	Silty Loam with Sand
1.0 m	5 YR 3/4	Dark Red Brown	Silty Loam
1.1 m	5 YR 3/3	Dark Red Brown	Silty Loam
1.2 m	5 YR 3/2	Dark Red Brown	Silty Loam with Clay and Sand
1.3 m	2.5 YR 3/1	Dark Red Gray	Silty Loam with Clay and Sand

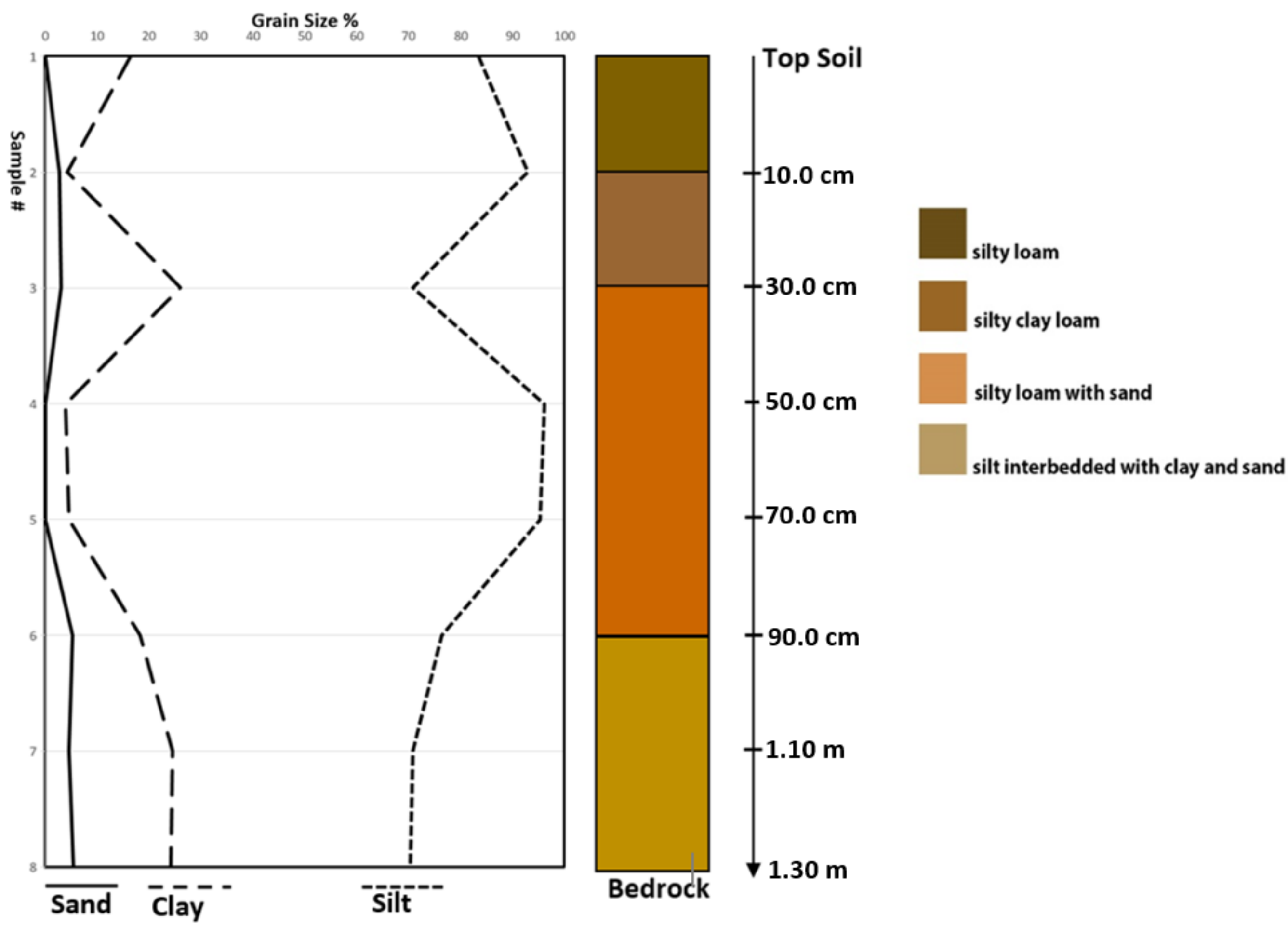

Figure 19: The Riverbank Profile of Lytle Creek along the river channel.

GPR Data Interpretation

The GPR data were interpreted based on visual examination of exposed sediments along the river channel and GPR reflections. Grids were denoted by letters A – G, with a maximum of 12 transects in each grids (Figure 20). Amidst all these transects, some were distorted due to interference with cables and the electrical problem of the equipment. However, a significant amount of transects were selected from each grids to interpret and explain the floodplain lithology and depositions in the study area.

Characterization and Interpretations of Reflection

Radar Facies

Three radar facies were found within all GPR profiles: horizontal-to-subhorizontal, curved upwardly concaved hyperbolic, and discontinuous (non-parallel) reflections (Table 3). Three radar facies were also recognized with some traces of hyperbolas showing indications of cables or pipes beneath the study area. Some data did not yield interpretable results, due to interference and attenuation of signals, however, a number of the GPR reflections were interpreted to show the floodplain and understand paleoflood depositions. The GPR profiles show significant reflection loss within 2 m of the surface as a result of the bedrock. It should be noted that some profiles contain poor reflection which extends from a distance of 2 m – 6 m. It is speculated that this is due to pavement and the concrete walkway in the area.

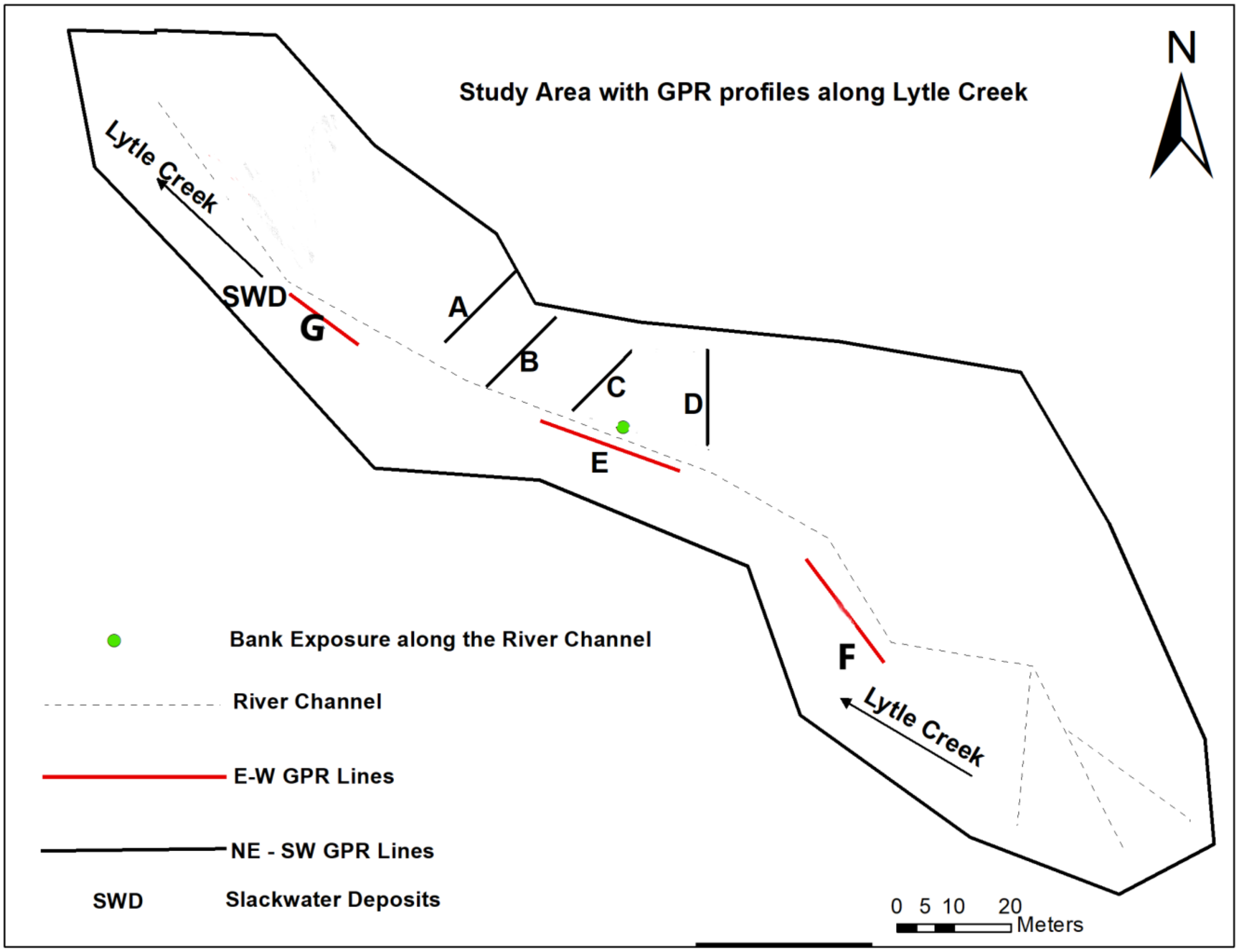

Figure 20: Map showing the location of the GPR profiles and the direction of the river channel.

Radar Facies I: Horizontal-to-sub horizontal reflections

Radar Facies (RF I) is approximately 10 – 30 cm, seen in most transects (Table 3). A number of these reflections along the profile also show a blend of parallel and hyperbolic reflections that might have been caused due to human activities in the environment (Okazaki et al., 2015). RF I is interpreted as being vertically accreted deposits from previous flooding events. The subparallel and wavy nature of deposition along the profile also is assumed to be from discontinuous bedload deposition (Hugenholtz et al., 2007).

Radar Facies II: Curved, upwardly concaved hyperbolic reflections

Radar Facies II (RF II) is analogous to RF I with few exceptions in the signature (Table 3). RF II is characterized by discontinuous to wavy reflections that can be traced for approximately 20 to 60 cm depth in some profiles. These reflections are evenly separated and wavy, and rarely continuous along the entire profile. RF II is most notable along the longitudinal section (Table 4). The reflections in RF II can be attributed to layers of silty loam and silty clay (Okazaki et al., 2015). RF II is interpreted to be vertically accreted flood depositions (Hickin et al., 2009). Okazaki et al., (2015) discussed that the undulating nature of the reflections might have resulted due to excessive rainfall that deposited the silty sand.

Radar Facies III

Radar Facies III (RF III) shows a discontinuous and oblique (non-parallel) reflections, and the lower boundary having faded reflections. It can be characterized as trough-shaped or curved concave reflections (Table 3). RF III's discontinuous reflections may be a proof of various types of deposits and is interpreted to consist of locally variable sediments such as trace of silt, silt loam, and silty clay with sand (Lunt et al., 2004). The other notable features can be interpreted as attenuation of the signals due to the bedrock.

Table 3: The diagnostic characteristics and depositional environments of the three radar facies.

Radar facies	GPR Image	Lithology	Interpretation
Radar facies I Horizontal-to-subhorizontal reflections	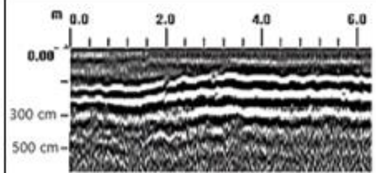	Silty Loam layers and Silty clay (dark to reddish brown)	Overbank Vertical Accretion deposits
Radar facies II Curved, upwardly concaved hyperbolic reflections	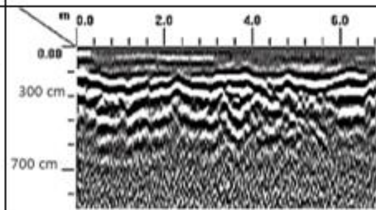	Silty loam with a little bit of sand	Lateral accretion, lateral migration of river, and erosional surfaces.
Radar facies III Discontinuous, irregular, and oblique reflections.	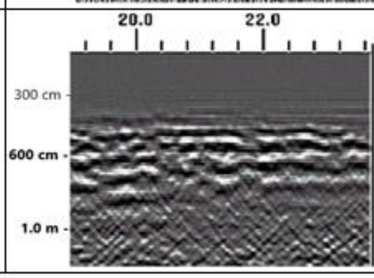	Silty loam and Silty clay	Deposits of bedrock.

Interpretations of Grids (Grid A - Grid G)

Grid A

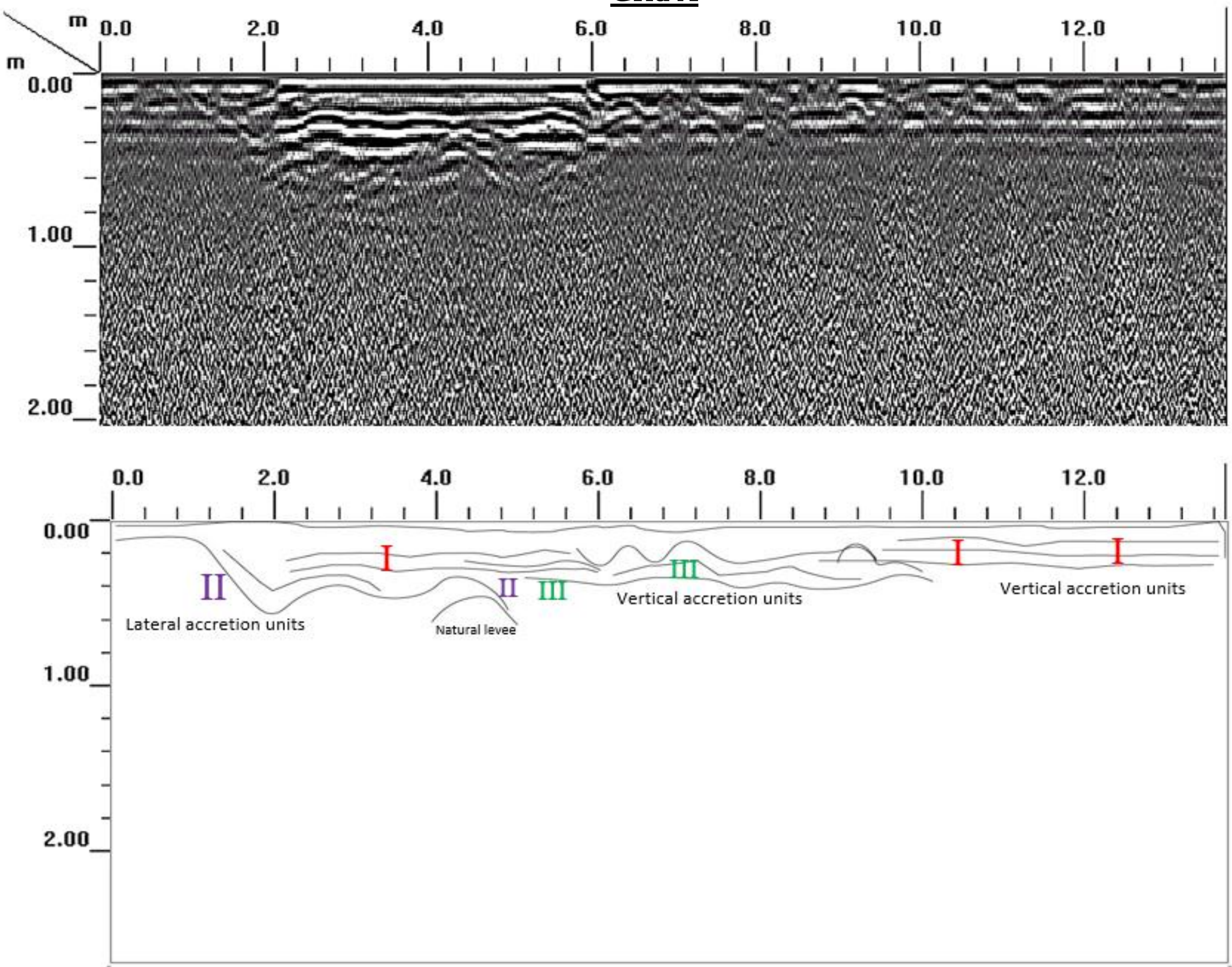

Figure 21: The reflection along Grid A (two transects were interpreted for this grid) *Note: red is RF I, pink is RF II, and green is RF III.*

Grid A (see Figure 20) along the river channel has RF I, II, and III. The interbedded unit is characterized by wavy and moderate reflections. This unit is abundant in the active river channel in the center part of the floodplain and noticeable up to 50 cm depth. The lateral accreted units can be noticed between 0 – 2 m of the profile. Parallel reflections (vertical accretion) indicate texturally fine silty loam materials with sand (Heteren et al., 1998). Grid A shows deposit of fine silty loam soil. Some of the horizontal profiles distinguished by the double thickness can be observed at 40 cm between 2 – 6 m. A total of 14 transects were derived from this grid which are shown in the appendix.

Grid B

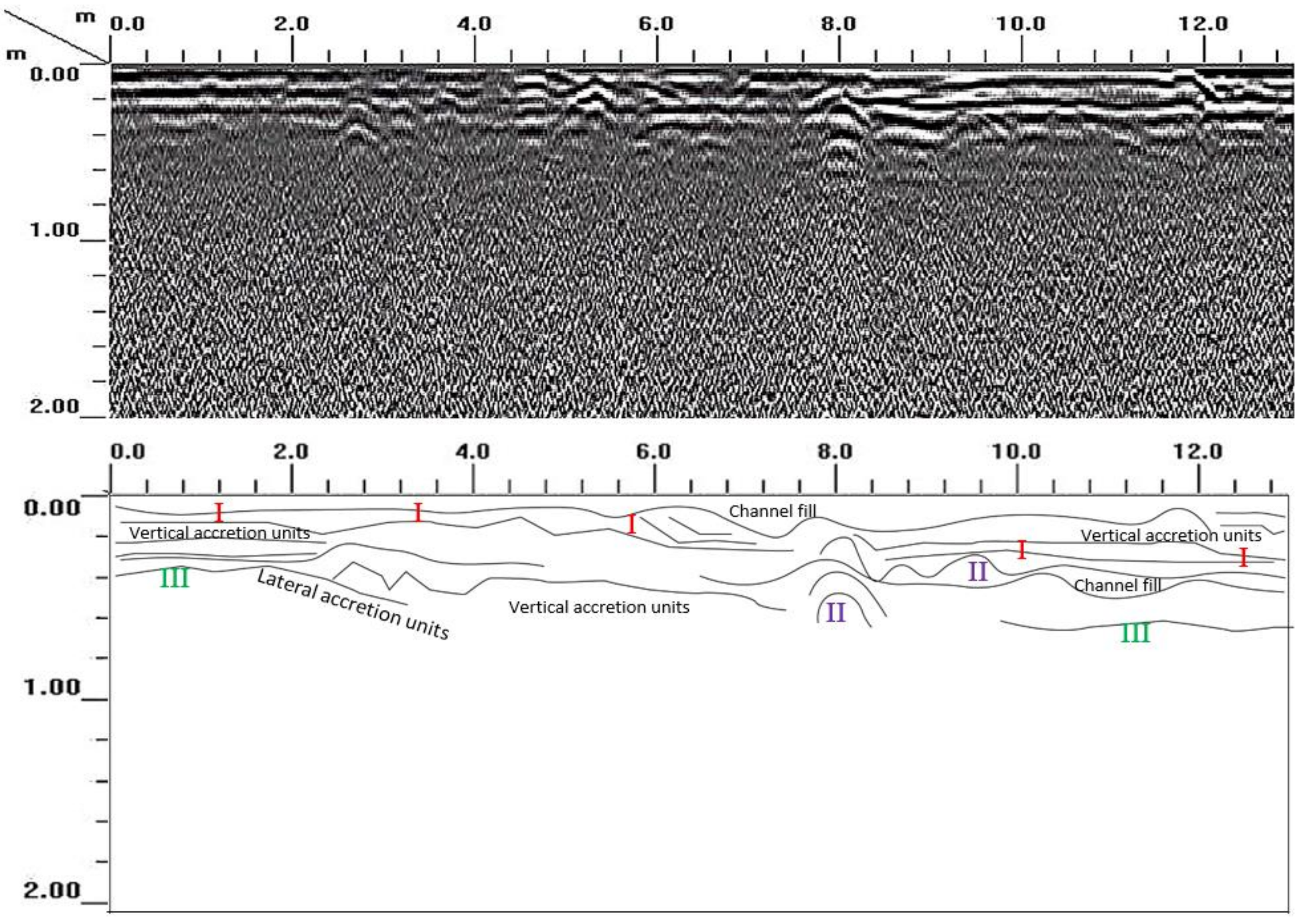

Figure 22: Representative GPR profile for Grid B and interpretation *Note: red is RF I, pink is RF II, and green is RF III.*

Grid B (see Figure 20) has sets of divergent, wavy, and slightly continuous reflection with a few high-to-low amplitude reflectors. The reflections on Grid B correlate with high silty loam soil seen on the riverbank profile occurring at 20 to 25 cm. The lower part of the reflection has a low reflection due to presence of silty loam with clayey material (Ekes and Hickin, 2001).

The upper layer has vertical accretion with channel fill at approximately 7 m reaching a depth 10 cm. The lower part of the profile at approximately 50 cm depth has lateral accretion which extends to 3 m. The entire profile has a blend of both vertical and lateral accreted depositions as indicated by RF I, RF II, and RF III.

<u>Grid C</u>

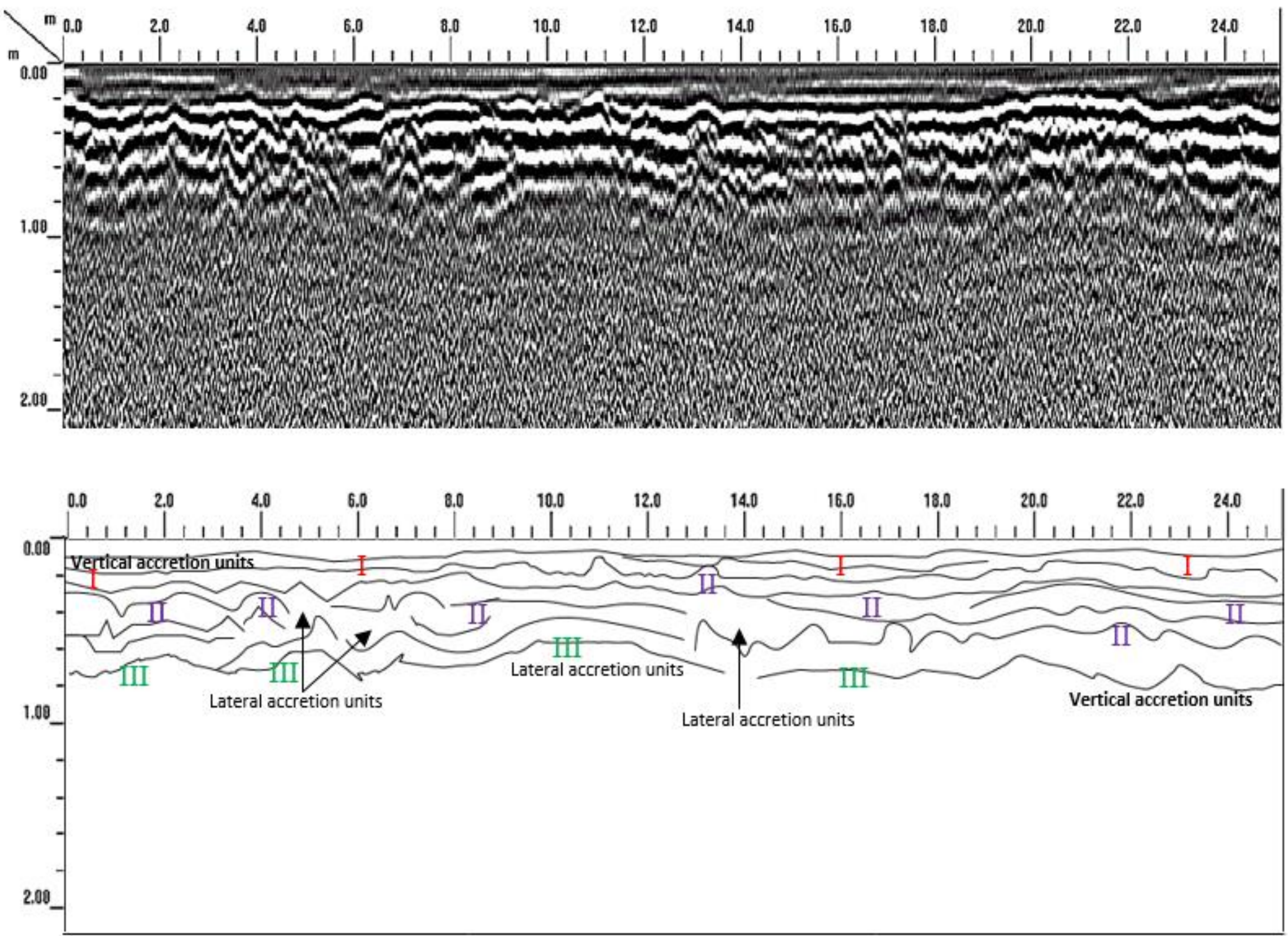

Figure 23: Representative GPR profile for Grid C and interpretation *Note: red is RF I, pink is RF II, and green is RF III.*

The reflections seen in Grid C has variable orientation with RF I and II being predominant (Figure 23). RF I and RF II in this profile shows layer of silty loam clay with sand at approximately 20 cm due to the upwardly concaved hyperbolic reflections that are exhibited in the upward sequence. There are traces of vertical accreted deposits toward the end of the profile. This profile can be described as lateral migration of the river channel (Kostic and Baker, 1988) or it could also mean lateral accretion (Ekes and Hickin, 2001). The reflections on Grid C can be traceable on Grid D.

Grid D

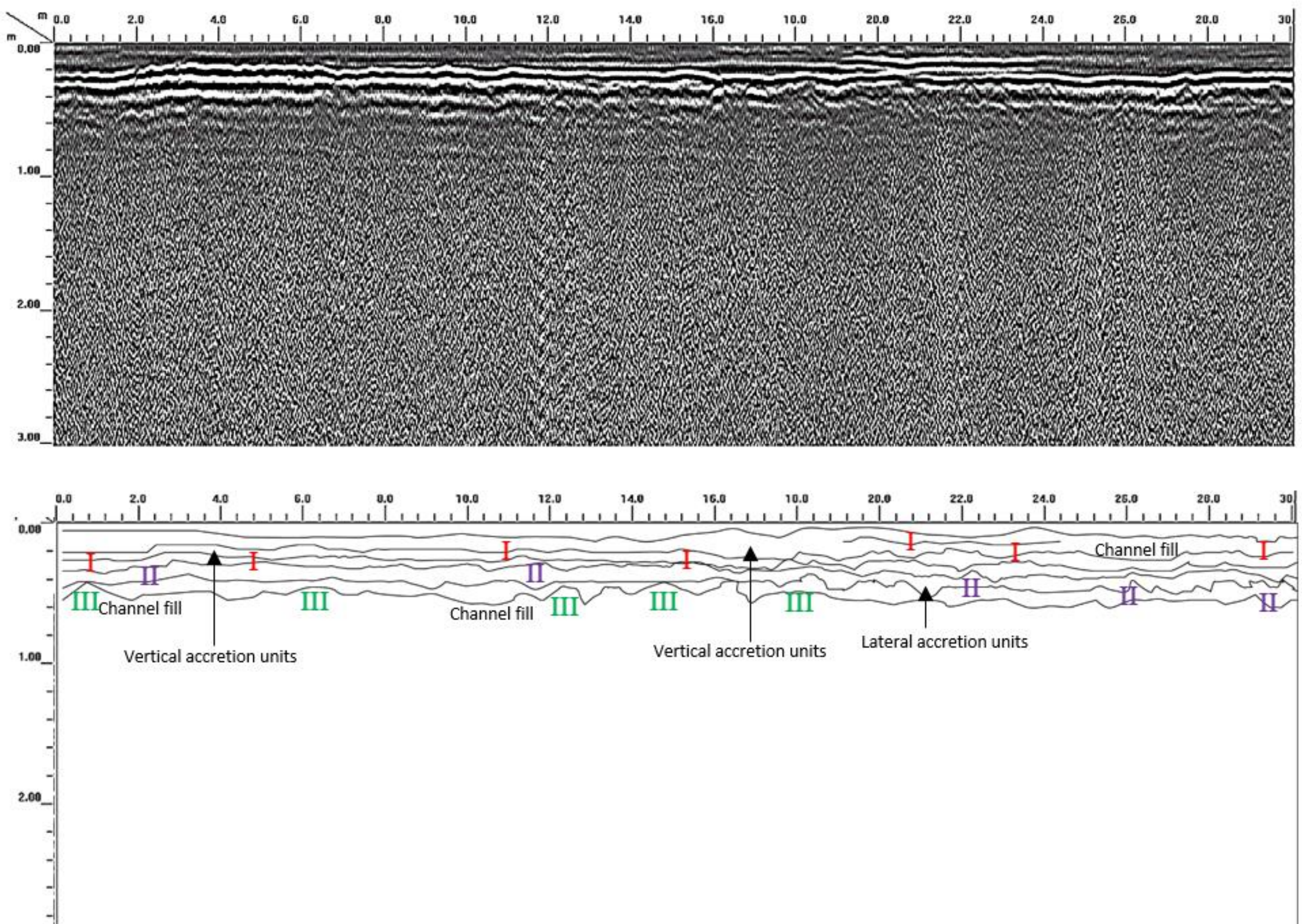

Figure 24: Representative GPR profile for Grid D and interpretation *Note: red is RF I, pink is RF II, and green is RF III.*

Grid D was taken close to the area where anthropogenic activities might have affected (Figure 20). This area has a high elevation compared to other areas selected for data acquisition. RF II is noted to be dominant within a depth of 20 to 50 cm, and extends to the entire profile. RF

II shows a strong, parallel, continuous, and hyperbolic reflections (Figure 22). Also, Grid D has a parallel geometry that undulating at the center of the profile which might indicate fillings. This undulation is noticeable between 12 – 14 m, and reaches a depth of 70 cm. The depth of penetration for this unit was dependent on the quantity of low permeability layers (clay and bedrock) which shows the channel fills (Figure 24). The existence of silty loam channel-fill in this floodplain area show that channel might have not been with filled clastic-materials and that it might not have experienced a high magnitude of flood (Dara, et al., 2018).

Grid E

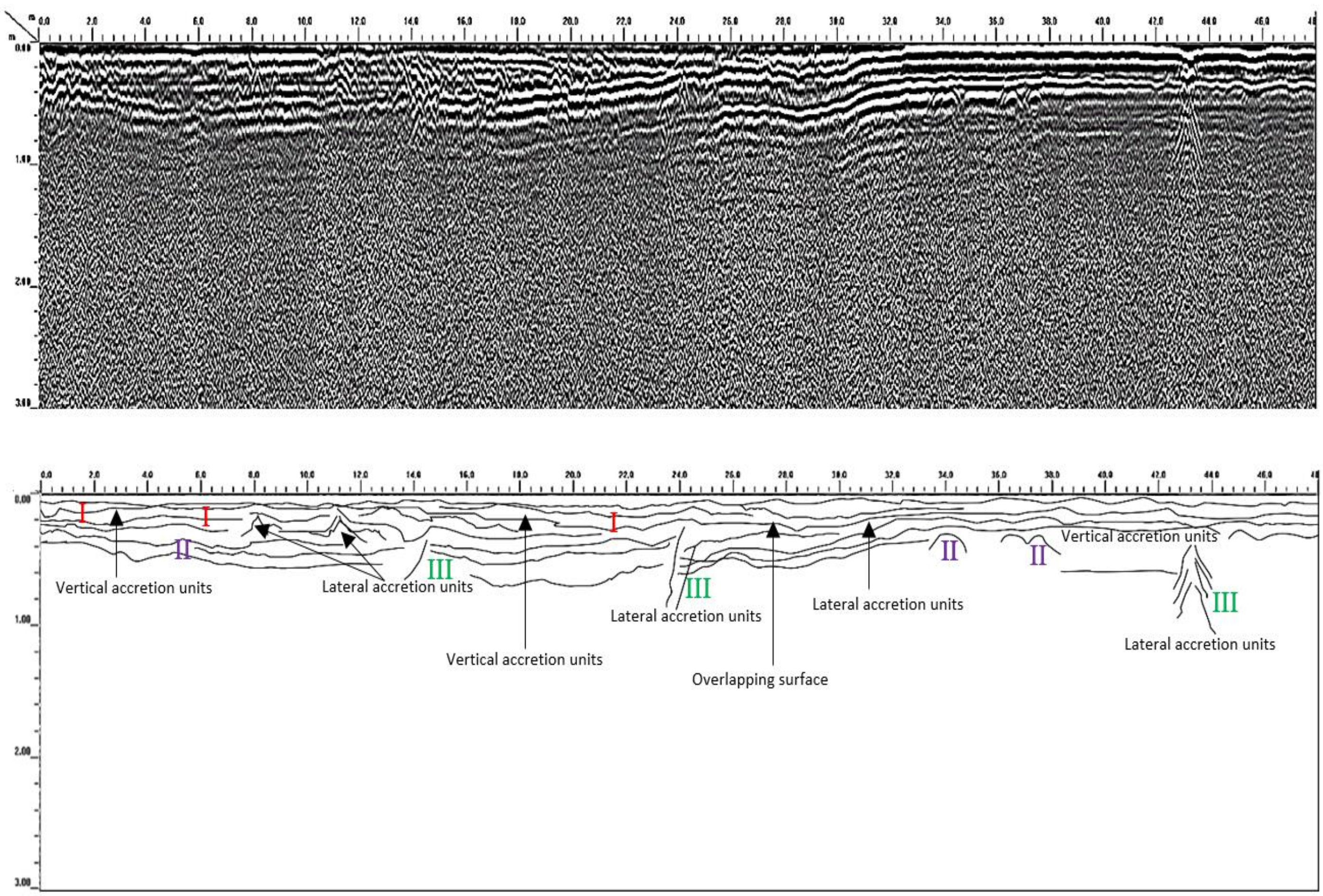

Figure 25: Representative GPR profile for Grid E and interpretation *Note: red is RF I, pink is RF II, and green is RF III.*

Grid E is close to the bank exposure (Figure 20). It was carried out to inspect for the results of the bank exposure analysis along the river channel. This profiles shows two or more layers, and with a length of 47 m. The overlapping surface can be seen between 18 to 34 m reaching a depth of 90 cm. The profile also consist layers having double horizontal, wavy, and parallel reflections which correlates with the results from the bank exposure (Figure 25). Vertical accreted depositions are seen in the top layers and lateral accretion are more predominant at the lower depth (Lunt et al., 2004; Dara, et al., 2018). The vertical accreted (RF I and II) and lateral accreted (RF III) layer can be interpreted to have silty clay loam and silty loam soil respectively which might represent pre-existing deposits (Jones et al., 2010). This interpretation correlates with the result of the grain size analysis (Figure 19).

Grid F

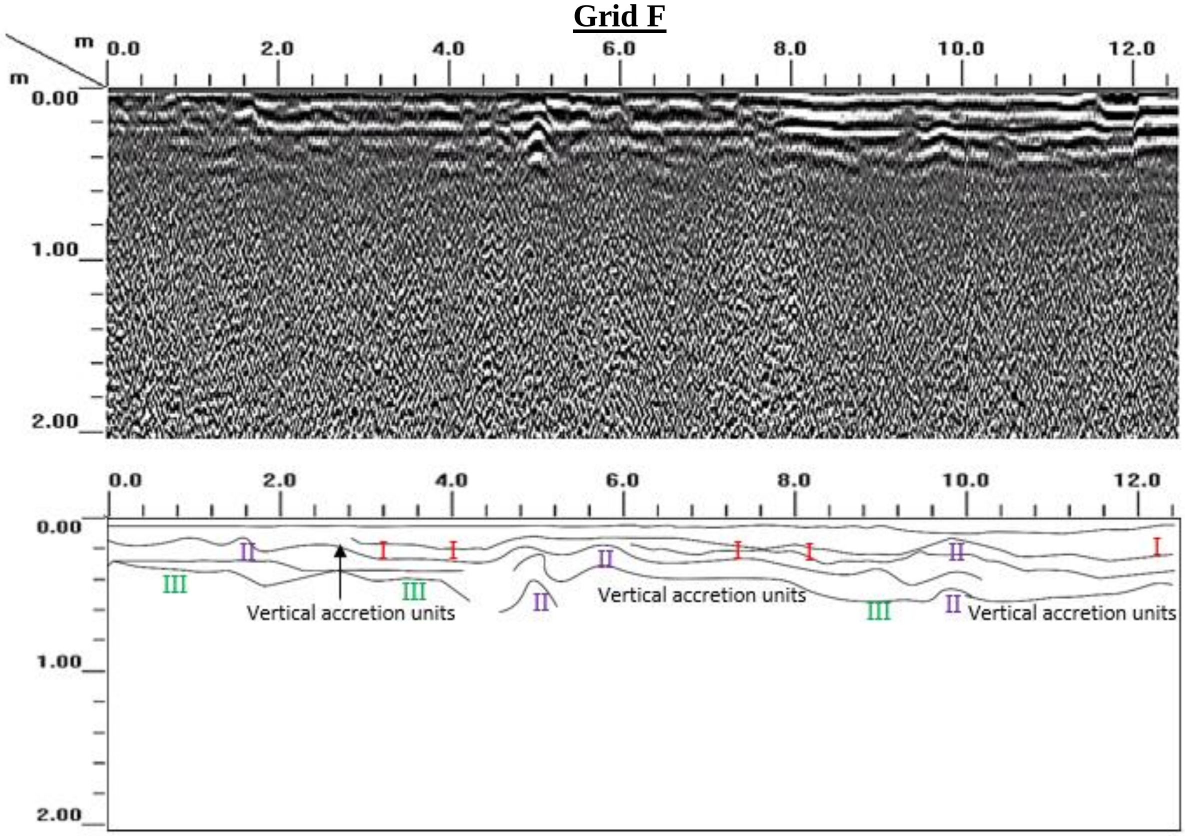

Figure 26: Representative GPR profile for Grid F and interpretation *Note: red is RF I, pink is RF II, and green is RF III.*

Grid F (see Figure 20) consists of wavy, sub-horizontal, and non-parallel reflections. RF I and II are more predominant and are vertically accreting in this profile (Figure 26). The middle part of the profile at 80 cm is analogous to silty loam deposits with mixtures of sand and clay as seen in the bank exposure analysis (Lunt et al., 2004; Dara, et al., 2018). Following the research by Jones et al., (2010), the sediments can be described to be vertically accreting as it progresses downward.

Grid G

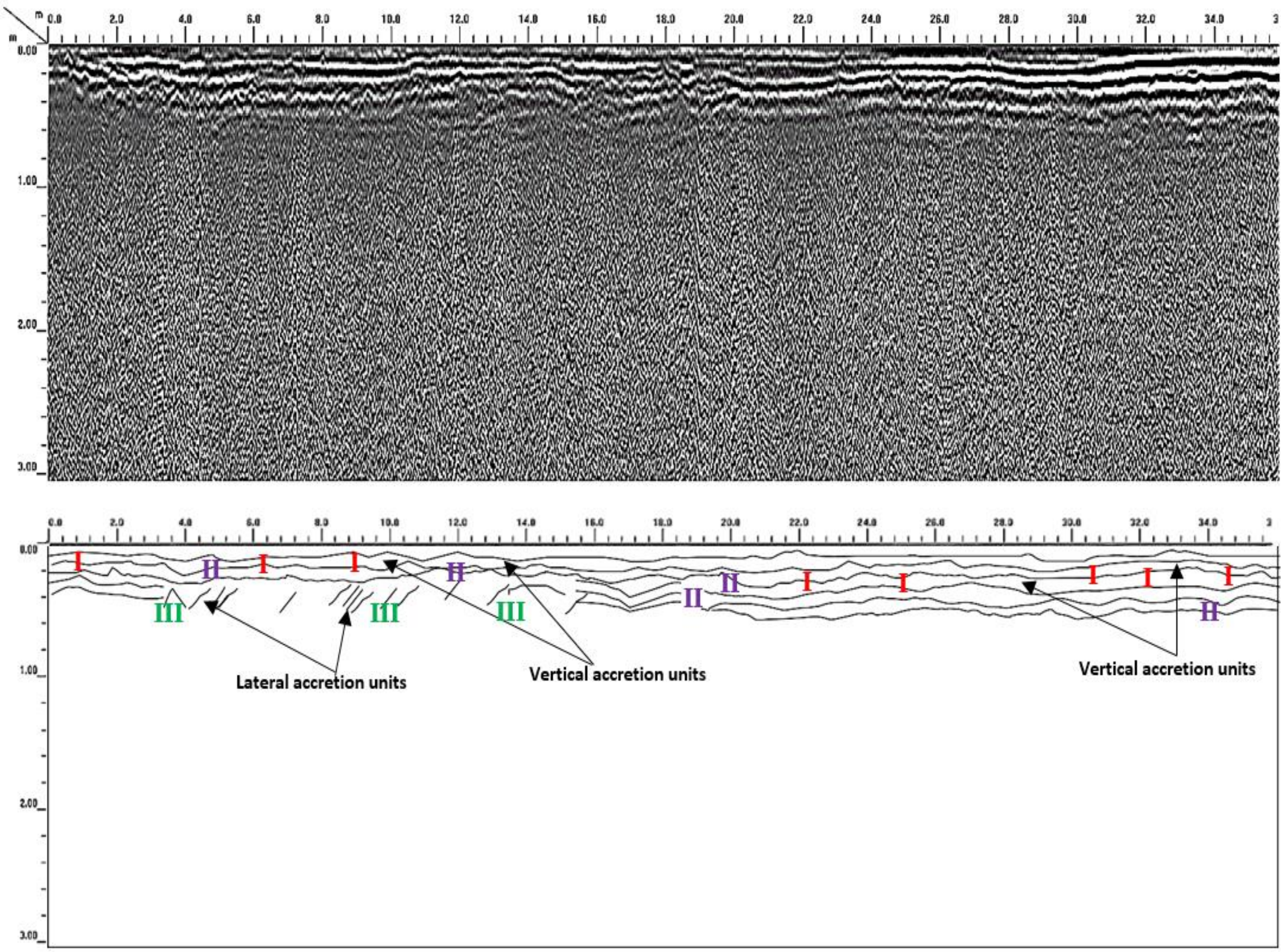

Figure 27: Representative GPR profile for Grid G and interpretation. *Note: red is RF I, pink is RF II, and green is RF III.*

Grid G (see Figure 20) was carried out close to the slackwater deposits (SWD) which shows large thickness between 24 to 36 m that reaches a depth of 50 cm. Investigating SWD is also a key to understand paleoflood history of the Lytle Creek. During high flood events, SWD accumulates in areas where there is reduction in flow velocity at channel expansions. The depositions mostly comprises fine sediments as indicated by RF I and RF II. RF III shows that the flood depositions are laterally accreting. There are a few undulating and hyperbolic reflections between 12 to 20 m which can be attributed to the presence of silty contents and are vertically accreting (Jones et al., 2010). At distance between 18 – 35 m, the horizontal and continuous reflections correspond to silty loam and silty clay deposits (Figure 27) (Dara et al., 2018; Leopold et al., 2006).

CHAPTER IV

DISCUSSION AND CONCLUSIONS

The sedimentological subsurface stratigraphy delineated at the studied area of Lytle Creek were homogenous at very small-scales (e.g. centimeter). To better understand geomorphological processes in the study area, the non-invasive GPR method was adopted with bank exposure analysis and guided different works found in the literature related to floodplain studies. The study demonstrates that GPR, GIS, and analysis of exposed sediments can help to understand sediment stratigraphy and the geometry of the texture in a lowland river. As a result, these methods can be recommended for subsurface stratigraphy studies in alluvial valley fills and for floodplain studies, because of relativity in imaging large areas.

Three major radar facies were obtained for the entire profile along Lytle Creek. RF I indicates horizontally and sub-horizontally reflections which might have been deposited during major flood events. The silty loam deposits were obvious in places where sediment-laden floodwaters had a decrease in flow as seen on Grid G, and through their sedimentological and morphological characteristics, they were said to be slackwater deposits (Baker, 1987; Leopold et al., 2006) (Figure 27). The selected transects for each grids have similarities in the way they are accreting i.e. vertical and lateral accretion. RF I can be noted to be vertically accreting where RF II and RF III are both vertically and laterally accreting. The lateral accretion, comprising silty loam and silty clay, were deposited close to grids long the bank exposure and mostly in the entire profile. This distribution suggests that only sediment-laden floods events might have caused these deposits (Leopold et al., 2006). Eitel et al., (2005), described that waning floods are noted not to transport large quantities of sediments, resulting in massive, well-sorted silt layers which was observed in most of the grids. The sediment depositions might be from the past floods in 1908, 1948, and 1975 which constituted floodplain. However, the silty layer is often a fertile soil which is good for growing crops. Also, accumulation of silty loam can promote water retention and air circulation.

RF II represents sediments accumulated by overland flow during flash floods and deposited during the waning stages (Dara et al., 2018). Also, RF II and III mark low conductivity layers in the study area which implies suspended load sediments deposited only under low-flow conditions as mud drapes over coarser clastic bedform (Dara et al., 2018). The suspended load deposits (silts, sands, and silty loam) were located throughout the entire grids and were distributed vertically and laterally with differences in thickness and reflections. The upper unit of the GPR profiles are composed of horizontal layers of fluvial silts and silty clay as seen in Grid B and Grid E. The lower part consists of undulating, subparallel, wavy, and hyperbolic reflections that were laterally accreting (Figure 25).

Conclusions

Lytle Creek is characterized as a low-energy, predominantly silty loam, and vertically accreting floodplain. GPR can help better understand floodplain development and evolution in Murfreesboro, Tennessee. Floodplain has advantages in providing floodwater storage, enhances biological productivity, habitat for fish and wildlife, and provides area of scientific study and outdoor education. This study was able to determine the paleoflood depositions and characterize the floodplain using GPR and bank exposure analysis. However, It should be noted that GPR solely be used to identify subsurface stratigraphy of Lytle Creek and the depositions of the fine silty floodplain. Integrating GPR techniques alongside other methods can help to visualize the horizontal and vertical distributions of sediments. GPR profiles cannot totally eliminate the usefulness of core samples, because each layer detected by GPR still needs to be verified in terms of their lithologic attributes. Future work need to be carried out at the study area involving soil probing at different locations. Statistical analysis can be carried out on the GPR data to show the area having concentration of silt formation. Radiometric dating of the samples using X-ray Fluorescence (XRF) can be done to determine the age and year of the floodplains.

BIBLIOGRAPHY

Adetunji, A.Q., Al-Shuhail, A., and Korvin, G., 2008. Mapping the internal structure of sand dunes with GPR: A case history from the Jafurah sand sea of eastern Saudi Arabia: The Leading Edge, v. 27, p. 1446–1452, doi: 10.1190/1.3011016.

Allen, J.R.L., 1965. A review of the origin and characteristics of recent alluvial sediments. Sedimentology, 89-191.

Annan, A.P., Davis, J.L., 1992. Design and development of a digital ground penetrating radar system. In: Pilon, J. (Ed.), Ground Penetrating Radar. Geol. Surv. Can. Pap. 90-4, 15–23.

Bakker, M., Maljers, D., and Weerts, H., 2007. Ground-penetrating radar profiling on embanked floodplains: Netherlands Journal of Geosciences - Geologie en Mijnbouw, v. 86, p. 55–61, doi: 10.1017/s0016774600021314.

Baker, V. R. (2008). Paleoflood hydrology: Origin, progress, prospects. Geomorphology, 101(1), 1–13. https://doi.org/10.1016/j.geomorph.2008.05.016

Beres, M. and Haeni, F. P. 1991. Application of ground-penetrating radar methods in hydrogeologic studies. *Ground Water,* 29, 375-386.

Bradley, M.W., and Hileman, G.E., 2006, Sinkhole flooding in Murfreesboro, Rutherford County, Tennessee, 2001-02: Scientific Investigations Report, doi: 10.3133/sir20055281.

Bridge, J.S., Alexander, J., Collier, R.E.L., Gawthorpe, R.L., Jarvis, J., 1995. Ground penetrating radar and coring used to study the large-scale structure of point-bar deposits in three dimensions. Sedimentology 42, 839–852.

Bristow, C.S., and Jol, H.M., 2003, An introduction to ground penetrating radar (GPR) in sediments: Geological Society, London, Special Publications, v. 211, p. 1–7, doi: 10.1144/gsl.sp.2001.211.01.01.

Collins, J. D., O’Grady, P., Langford, R. P., & Gill, T. E. (2016). End-Member Mixing Analysis (EMMA) Applied to Sediment Grain Size Distributions to Characterize Formational Processes of the Main Excavation Block, Unit 2, of the Rimrock Draw Rockshelter (35HA3855), Harney Basin, Eastern Oregon (USA). *Archaeometry*, *59*(2), 331–345. https://doi.org/10.1111/arcm.12243

Costa, J. E. (1978). Holocene stratigraphy in flood frequency analysis. Water Resources Research, 14(4), 626–632.

Dara R., Kettridge N., Rivett M.O., Identification of floodplain and riverbed sediment heterogeneity in a meandering UK lowland stream by ground penetrating radar, *Journal of Applied Geophysics*(2018), https://doi.org/10.1016/j.jappgeo.2019.103863.

Eitel, B., Kadereit, A., Blu¨ mel, W.D., Hu¨ ser, K. & Kromer, B. 2005. The Amspoort Silts, northern Namib desert (Namibia): formation, age and palaeoclimatic evidence of river-end deposits. Geomorphology, 64, 299–314.

Ekes, C., Hickin, E.J., 2001. Ground penetrating radar facies of the paraglacial Cheekye Fan, southwestern British Columbia, Canada. Sediment. Geol. 143, 199– 217.

Ekes, C., Friele, P., 2003. Sedimentary architecture and post-glacial evolution of Cheekye fan, southwestern British Columbia, Canada. In: Bristow, C.S., Jol, H.M. (Eds.), Ground Penetrating Radar in Sediments. Geol. Soc. London Spec. Publ. 211, 87– 98.

Ely, L. L., Webb, R. H., & Enzel, Y. (1992). Accuracy of post-bomb 137Cs and 14C in dating fluvial deposits. Quaternary Research, 38(2), 196–204.

Evans, R.D., 2009, Optimizing Ground Penetrating Radar (GPR) to Assess Pavements, Centre for Innovative and Collaborative Construction Engineering: https://www.lboro.ac.uk/research/cice/alumni/2010/dr-robert-evans.html (accessed December 2019).

Federal Emergency Management Agency, 1999, Flood insurance study, Rutherford County, Tennessee: Washington, D.C., Federal Emergency Management Agency, 135 p.

Harari, Z., 1996, Ground-penetrating radar (GPR) for imaging stratigraphic features and groundwater in sand dunes: Journal of Applied Geophysics, v. 36, p. 43–52, doi: 10.1016/s0926-9851(96)00031-6.

Heinz, J., Aigner, T., 2003. Three-dimensional GPR analysis of various Quaternary gravel-bed braided river deposits (southwestern Germany). In: Bristow, C.S., Jol, H.M. (Eds.), Ground Penetrating Radar in Sediments. Geol. Soc. London Spec. Publ.

Heteren, S., Fitzgerald, D., Mckinlay, P., & Buynevich, I. (1998). Radar facies of paraglacial barrier systems: coastal New England, USA. *Sedimentology*, *45*(1), 181-200. doi: 10.1046/j.1365-3091.1998.00150.x

Hickin, A.S., Kerr, B., Barchyn, T.E., Paulen, R.C., 2009. Using ground-penetrating radar and capacitively coupled resistivity to investigate 3-D fluvial architecture and grain-size distribution of a gravel floodplain in Northeast British Columbia, Canada. Journal of Sedimentary Research 79, 457–477.

Hugenholtz, C.H., Paulen, R.C., and Wolfe, S.A., 2007: Ground-penetrating radar investigation of relict channel bars of the Meander River spillway, northern Alberta; Geological Survey of Canada, Current Research 2007-A1, 10p. 211, 99–110.

Jackson, R. G., 1978. Hierarchical attributes and a unifying model of bed forms composed of cohesionless material and produced by shearing flow. Geological Society of America Bulletin 86, 1523-1533.

Jones, A.J., Heal, K.V., Stuart, N., Wallis, S.G., Lunn, R.J., and Barbara, B., (2007). Quantifying sediment deposition and the spatial variability of sediment-associated metals in ponds treating urban diffuse pollution. IAHS-AISH Publication, https://www.geos.ed.ac.uk/homes/kheal/jones_iugg_2007.pdf, v. 314. (Accessed December 2019).

Jones, A., Lewin, J., & Macklin, M. (2010). Flood series data for the later Holocene: Available approaches, potential and limitations from UK alluvial sediments. *The Holocene*, *20*(7), 1123–1135. https://doi.org/10.1177/0959683610369501

Kochel, R. C., & Baker, V. C. (1982). Paleoflood hydrology. Science, 215, 353–361.

Kochel, R. C., & Baker, V. R. (1988). Paleoflood analysis using slackwater deposits. In V. R. Baker, R. C. Kochel, & P. C. Patton (Eds.), Flood geomorphology (pp. 169–187). New York, NY: John Wiley & Sons.

Kowalsky, M., Finsterle, S., & Rubin, Y. (2004). Estimating flow parameter distributions using ground-penetrating radar and hydrological measurements during transient flow in the vadose zone. *Advances In Water Resources*, *27*(6), 583-599. doi: 10.1016/j.advwatres.2004.03.003

Law, G.S., 2002, Duration and Frequency Analysis of Lowland Flooding in Western Murfreesboro, Rutherford County, Tennessee, 1998-2000: U.S. Geological Survey Water-Resources Investigations Report 02-4266, p. 30, doi: 10.3133/wri024266.3396.

Leopold, M., Völkel, J., & Heine, K. (2006). A ground-penetrating radar survey of late Holocene fluvial sediments in NW Namibian river valleys: characterization and comparison. *Journal Of The Geological Society*, *163*(6), 923-936. doi: 10.1144/0016-76492005-092.

Lunt, I.A., Bridge, J.S., Tye, R.S., 2004. A quantitative, three-dimensional depositional model of gravelly braided rivers. Sedimentology 51, 377–414.

Nanson, G.C., 1986. Episodes of vertical accretion and catastrophic stripping: a mode of disequilibrium floodplain development. Bull. Geol. Soc. Am., 97: 1467-1475.

Nanson, G., & Croke, J. (1992). A genetic classification of floodplains. *Geomorphology*, *4*(6), 459-486. doi: 10.1016/0169-555x(92)90039-q

Neal, A., Roberts, C.L., 2000. Applications of ground-penetrating radar (GPR) to sedimentological, geomorphological and geoarchaeological studies in coastal environments. In: Pye, K., Allen, J.R.L. (Eds.), Coastal and Estuarine Environments: Sedimentology, Geomorphology and Geoarchaeology. Geol. Soc. London Spec. Publ. 175, 139– 171.

Neal, A. (2004). Ground-penetrating radar and its use in sedimentology: principles, problems and progress. *Earth-Science Reviews*, *66*(3-4), 261-330. doi: 10.1016/j.earscirev.2004.01.004

Okazaki, H., Kwak, Y., & Tamura, T. (2015). Depositional and erosional architectures of gravelly braid bar formed by a flood in the Abe River, central Japan, inferred from a three-dimensional ground-penetrating radar analysis. *Sedimentary Geology*, *324*, 32-46. doi: 10.1016/j.sedgeo.2015.04.008

Olhoeft, G.R., 1999. Applications and frustrations in using ground penetrating radar. Proceedings Ultra Wideband Conference, Washington DC, 20–22 September 1999.'

Pellicer, X., & Gibson, P. (2011). Electrical resistivity and Ground Penetrating Radar for the characterisation of the internal architecture of Quaternary sediments in the Midlands of Ireland. *Journal Of Applied Geophysics*, *75*(4), 638-647. doi: 10.1016/j.jappgeo.2011.09.019.

Radzevicius, S.J., Guy, E.D., and Daniels, J.J. 2000. Pitfalls in GPR data interpretation: differentiating stratigraphy and buried objects from periodic antenna and target effects. Geophysical Research Letters, vol. 27. 20: 3393-3396.

Riley, P., and Johnson, B. J. 2004, Historic hill cemetery – does it contain remains of General Anthony Wayne's Cantonment at Legion Ville. Proceeding of The Society for Pennsylvania Archaeology, 75th Annual Meeting, USA, p. 9.

Ronen, A., Ezersky, M., Beck, A., Gatenio, B., and Simhayov, R.B., 2019, Use of GPR method for prediction of sinkholes formation along the Dead Sea Shores, Israel: Geomorphology, v. 328, p. 28–43, doi: 10.1016/j.geomorph.2018.11.030.

Spicer, K.R., Costa, J.E., 1997, Measuring flood discharge in unstable stream channels using ground-penetrating radar: Geology, v. 25, p. 423, doi: 10.1130/0091-7613(1997)025<0423: mfdius>2.3.co; 2.

Stedinger, J. R., & Cohn, T. A. (1986). Flood frequency analysis with historical and Paleoflood information. Water Resources Research, 22, 785–793. https://doi.org/10.1029/WR022i005p00785

Stephanie, V. (2007). Paleoflood record reconstruction at an archaeological site on the Owyhee River, southeastern Oregon. Central Washington University.

Thornberry-Ehrlich, T. L. 2012. Stones River National Battlefield: Geologic resources inventory report. Natural Resource Report NPS/NRSS/GRD/NRR—2012/566. National Park Service, Fort Collins, Colorado.

Tischler, M.E., Collins, M.E., and Grunwald, S.E., 2002, Integration of ground-penetrating radar data, global positioning systems, and geographic information systems to create three-dimensional soil models: Ninth International Conference on Ground Penetrating Radar, doi: 10.1117/12.462302.

Tsoflias, G. P., and Becker, W. B., 2008, Ground-penetrating-radar response to fracture-fluid salinity: Why lower frequencies are favorable for resolving salinity changes. Geophysics, v. 73, p. 25–30, doi: 10.1190/1.2957893.

USDA, 1977, (U.S. Department of Agriculture, Soil Conservation Service), Soil survey of Rutherford County, Tennessee: Washington, D.C., U.S. Department of Agriculture, p. 95.

U.S. Army Corps of Engineers, 1966, Main report—Flood plain information study, West Fork Stones River, Lytle and Sinking Creeks, Murfreesboro, Tennessee: Nashville, Tennessee, U.S. Army Corps of Engineers, p. 45.

USGS WaterWatch 2020 -- streamflow conditions. (n.d.). From https://waterwatch.usgs.gov/new/index.php?mt=floodz&st=Murfreesboro&usst=&ushuc=&id=wwlmap_viewer Retrieved March 12, 2021,

Utsi, E., 2006, Ground-penetrating radar for archaeology. Lawrence B. Conyers. AltaMira Press, Walnut Creek, California, 2004. 203pp. ISBN 0-759-10773-4: Archaeological Prospection, v. 13, p. 228–229, doi: 10.1002/arp.288.

Wilhelm B, Ballesteros Cánovas JA, Macdonald N, et al. Interpreting historical, botanical, and geological evidence to aid preparations for future floods. WIREs Water. 2019;6:e1318. https://doi.org/10.1002/ wat2.1318.

Wolf, L.W., Collier, J., Tuttle, M., and Bodin, P., 1998, Geophysical reconnaissance of earthquake-induced liquefaction features in the New Madrid seismic zone: Journal of Applied Geophysics, v. 39, p. 121–129, doi:https://doi.org/10.1016/S0926-9851 (98)00016-0.

Woodward, J., Ashworth, P. J., Best, J. L., Sambrook Smith, G. H. & SIMPSON, C. J. 2003. The use and application of GPR in sandy fluvial environments: methodological considerations. In: Bristow, C. S. & Jol, H. M. (eds) Ground Penetrating Radar in Sediments. Geological Society, London, Special Publications, 211, 127-142.

Wright, E.P.E., 2019, Alternative Uses of Ground Penetrating Radar in Highway in Construction and Maintenance, Transportation.org: https://research.transportation.org/wp-content/uploads/sites/31/2017/08/HVR-Arkansas.pdf (accessed December 2019).

APPENDICES

Appendix A

GPR Radar Profiles

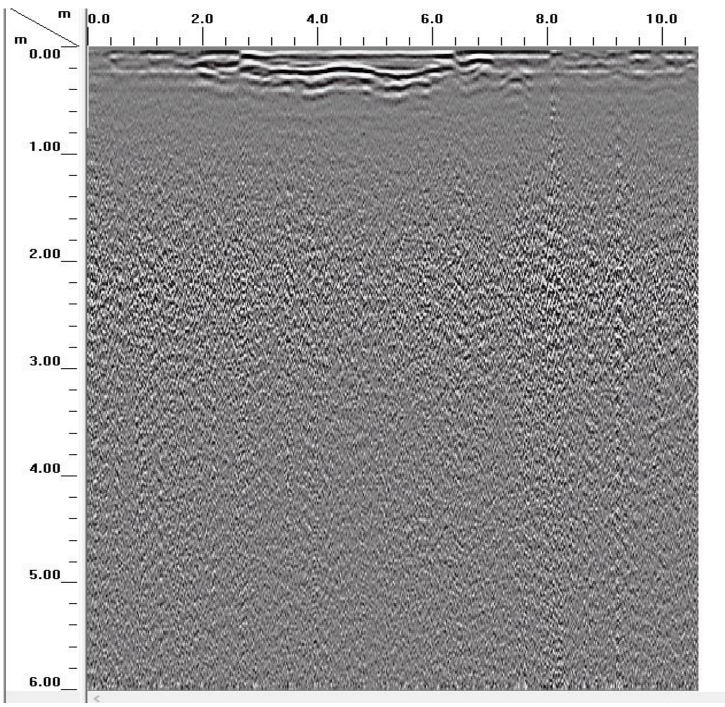

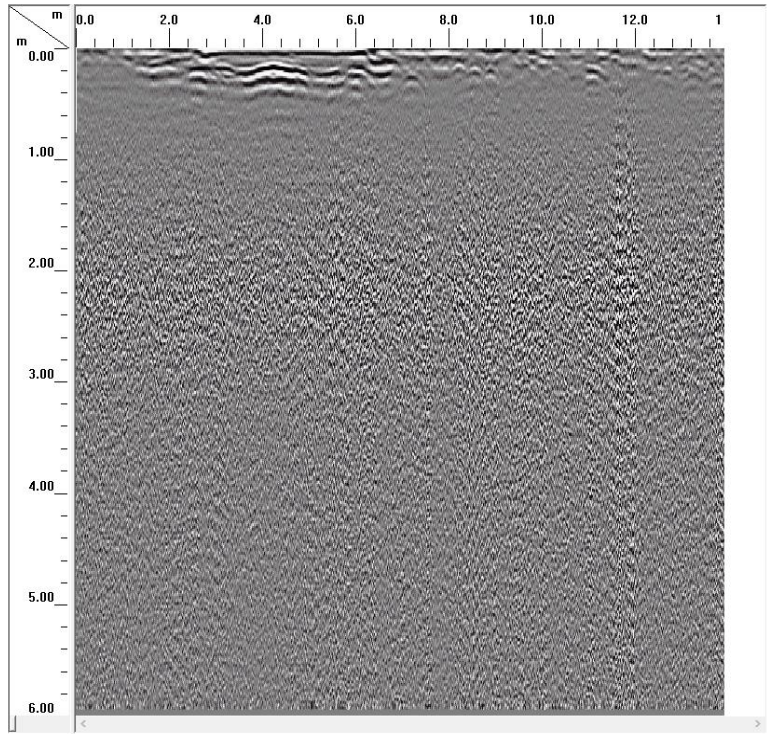

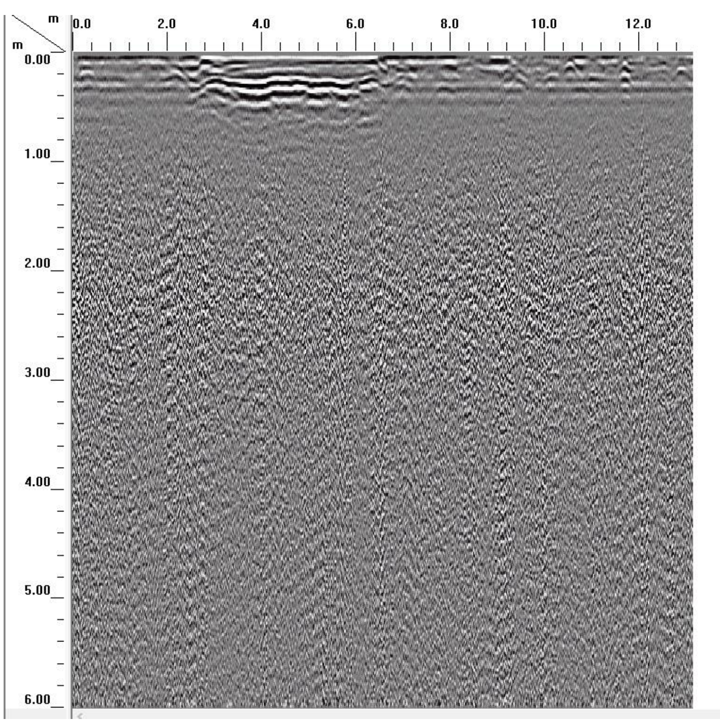

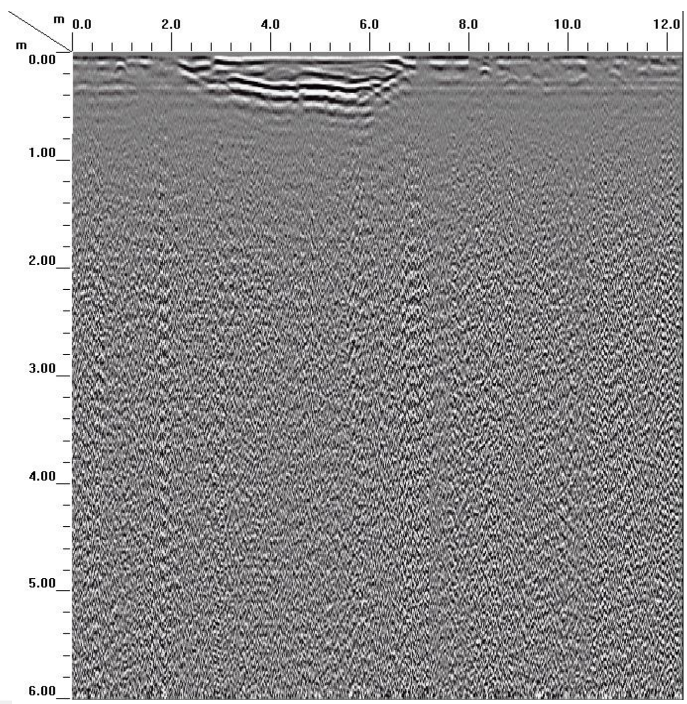

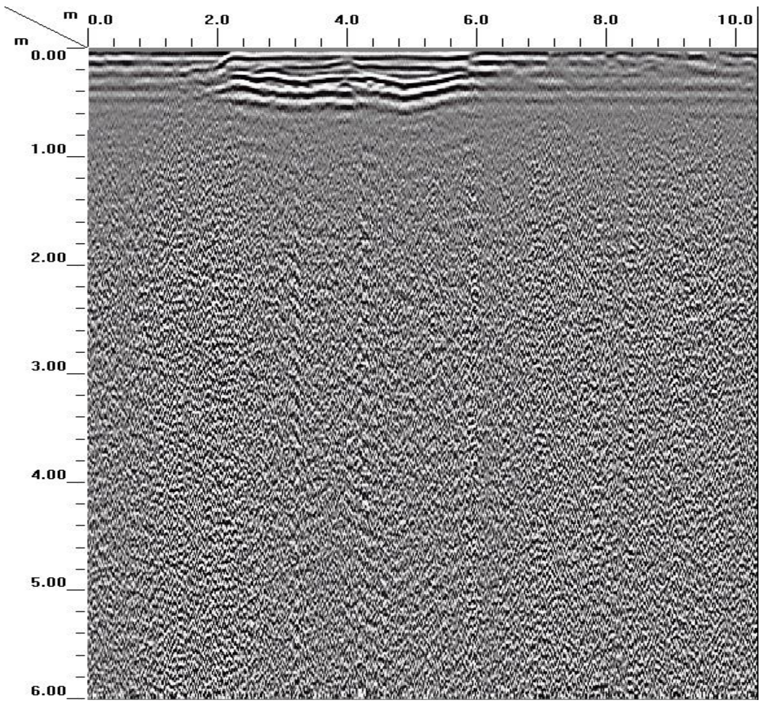
m
m
0.0
2.0
4.0
6.0
8.0
10.0
0.00
1.00
2.00
3.00
4.00
5.00
6.00

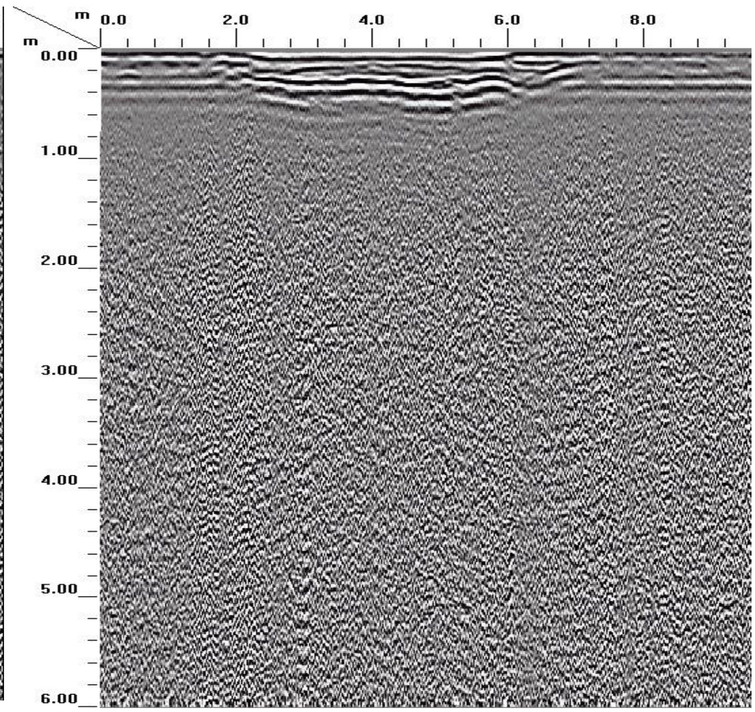
m
m
0.0
2.0
4.0
6.0
8.0
0.00
1.00
2.00
3.00
4.00
5.00
6.00

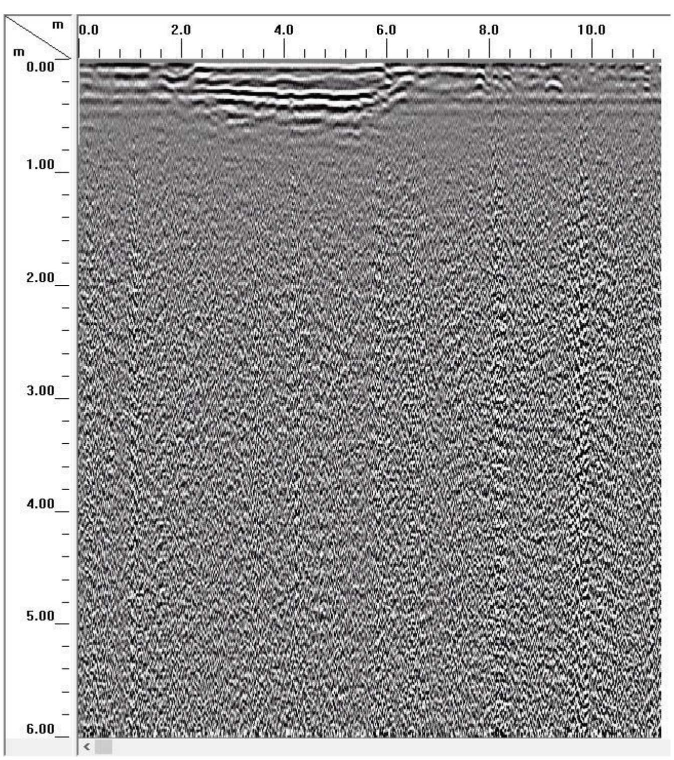
m
m
0.0
2.0
4.0
6.0
8.0
10.0
0.00
1.00
2.00
3.00
4.00
5.00
6.00

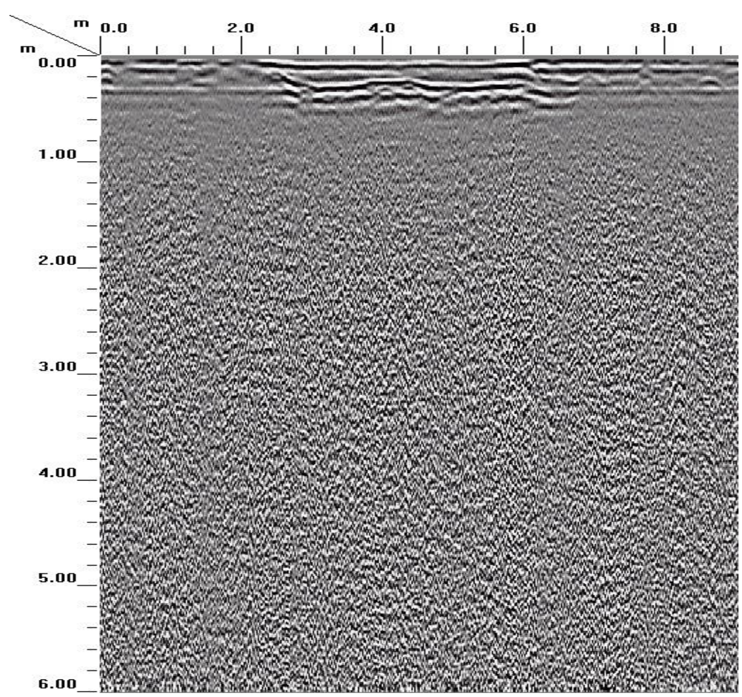
m
m
0.0
2.0
4.0
6.0
8.0
0.00
1.00
2.00
3.00
4.00
5.00
6.00

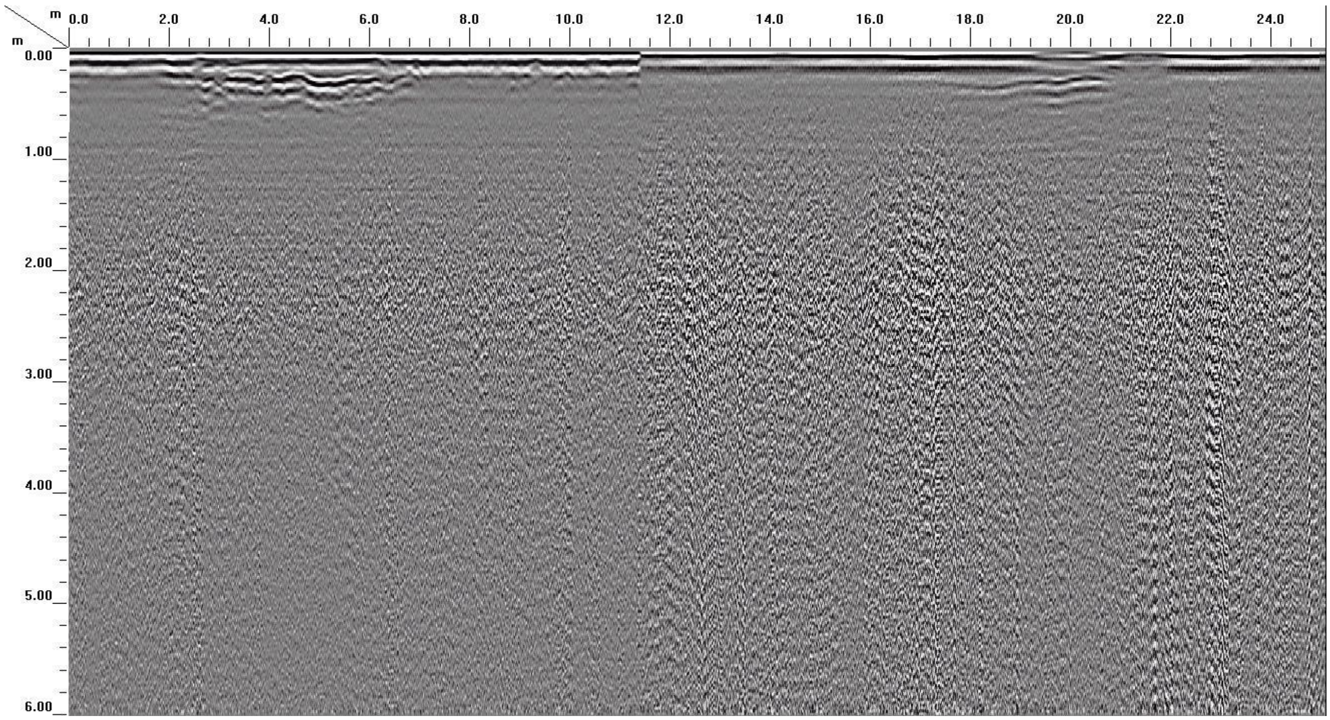

Figure B1: GPR profiles for GRID A (line 3 – 14).

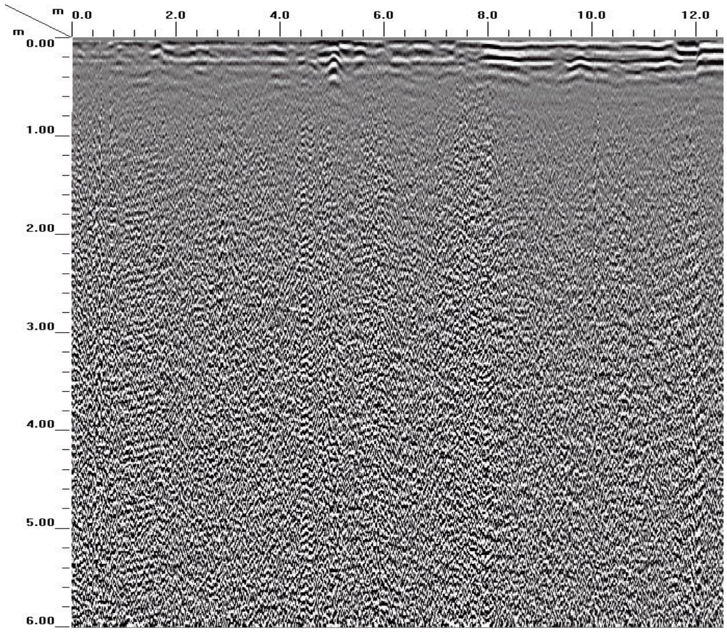

m
0.0
2.0
4.0
6.0
8.0
10.0
12.0
0.00
1.00
2.00
3.00
4.00
5.00
6.00

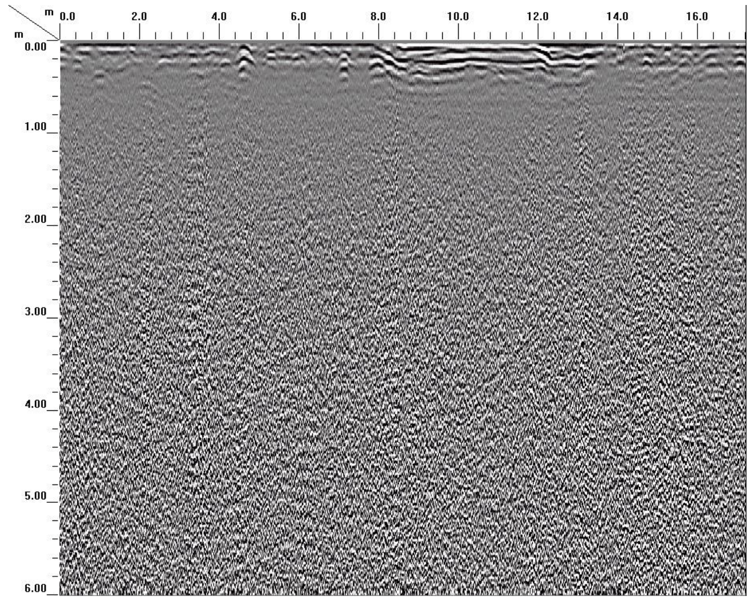

m
0.0
2.0
4.0
6.0
8.0
10.0
12.0
14.0
16.0
0.00
1.00
2.00
3.00
4.00
5.00
6.00

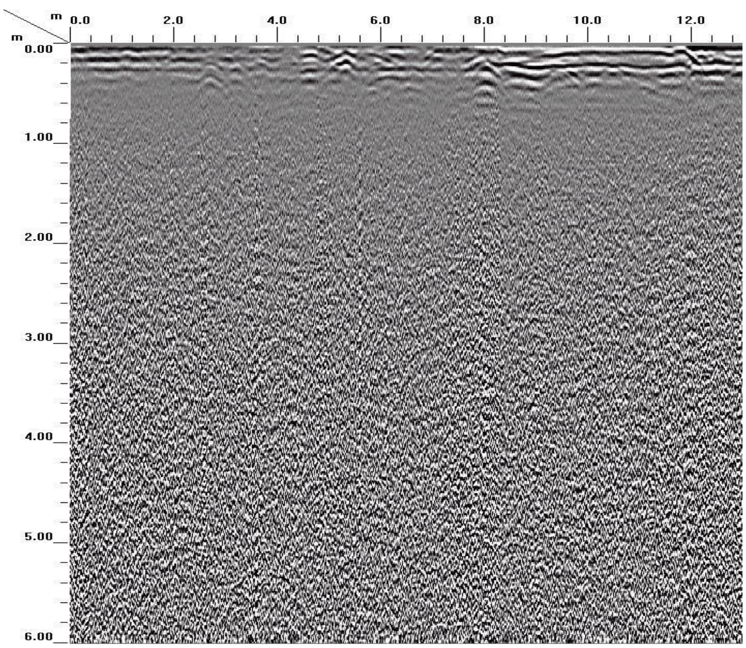

m
0.0
2.0
4.0
6.0
8.0
10.0
12.0
0.00
1.00
2.00
3.00
4.00
5.00
6.00

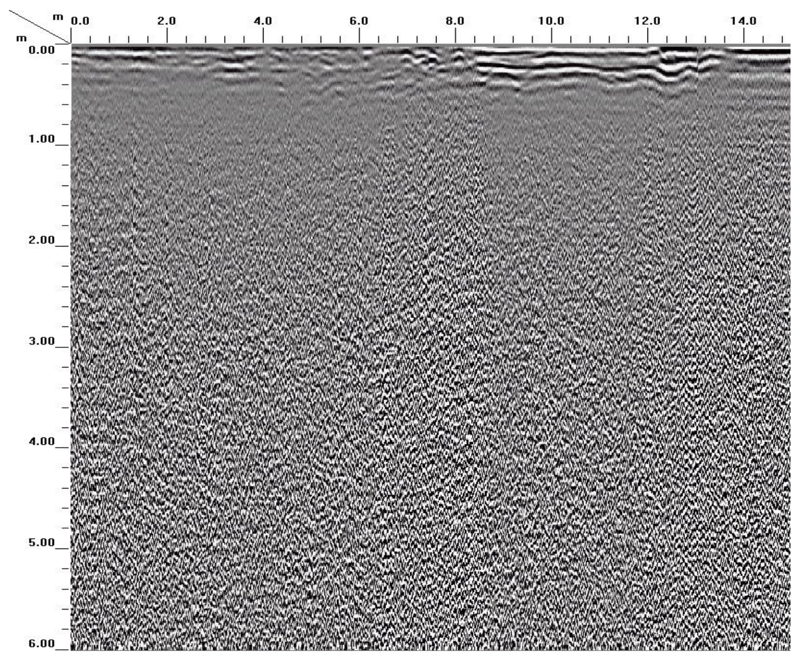

m
0.0
2.0
4.0
6.0
8.0
10.0
12.0
14.0
0.00
1.00
2.00
3.00
4.00
5.00
6.00

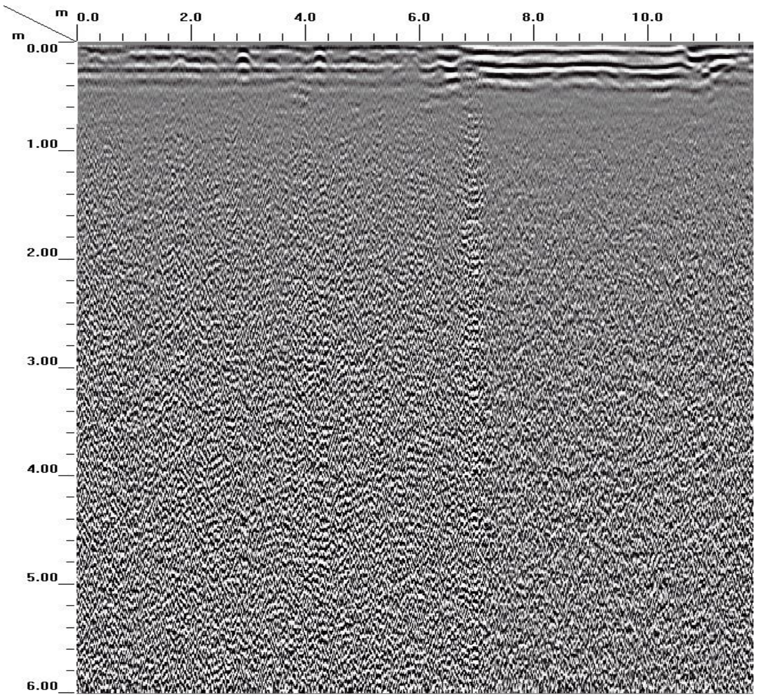
m
0.0
2.0
4.0
6.0
8.0
10.0
m
0.00
1.00
2.00
3.00
4.00
5.00
6.00

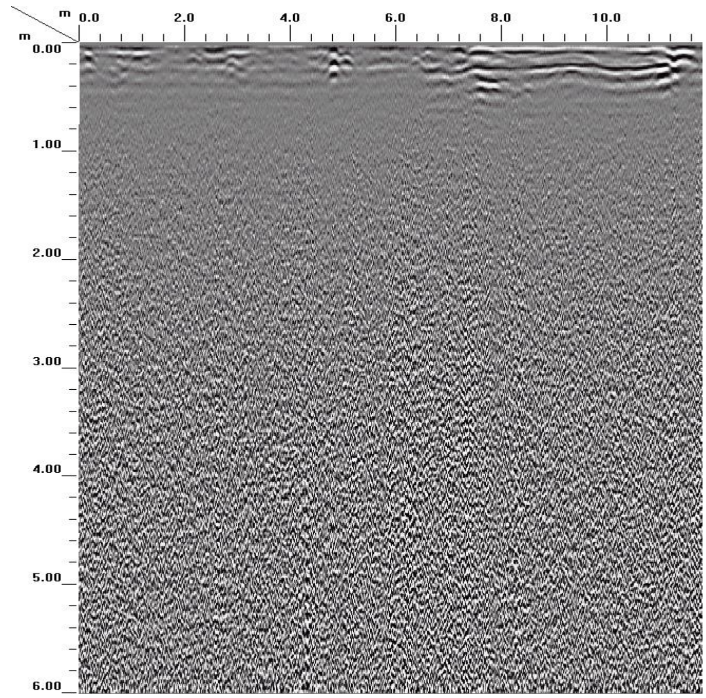
m
0.0
2.0
4.0
6.0
8.0
10.0
m
0.00
1.00
2.00
3.00
4.00
5.00
6.00

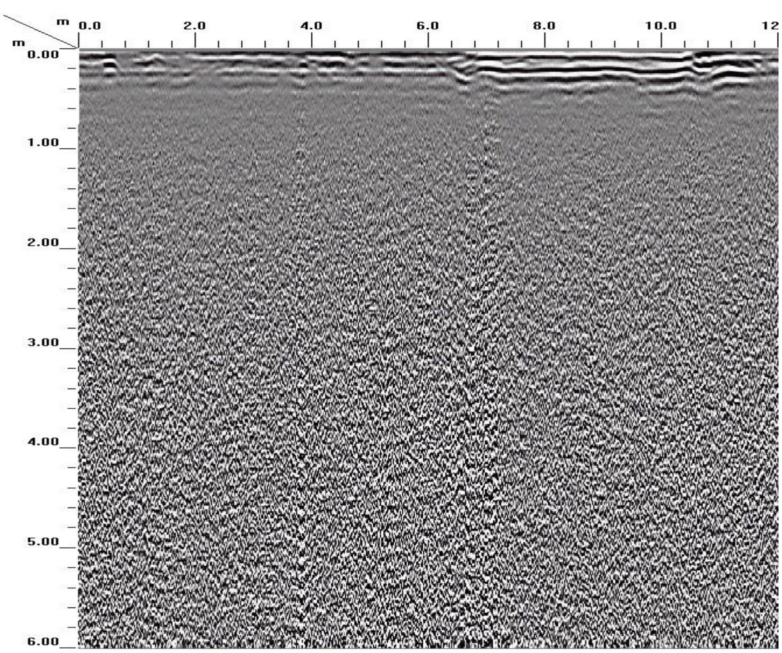
m
0.0
2.0
4.0
6.0
8.0
10.0
12
m
0.00
1.00
2.00
3.00
4.00
5.00
6.00

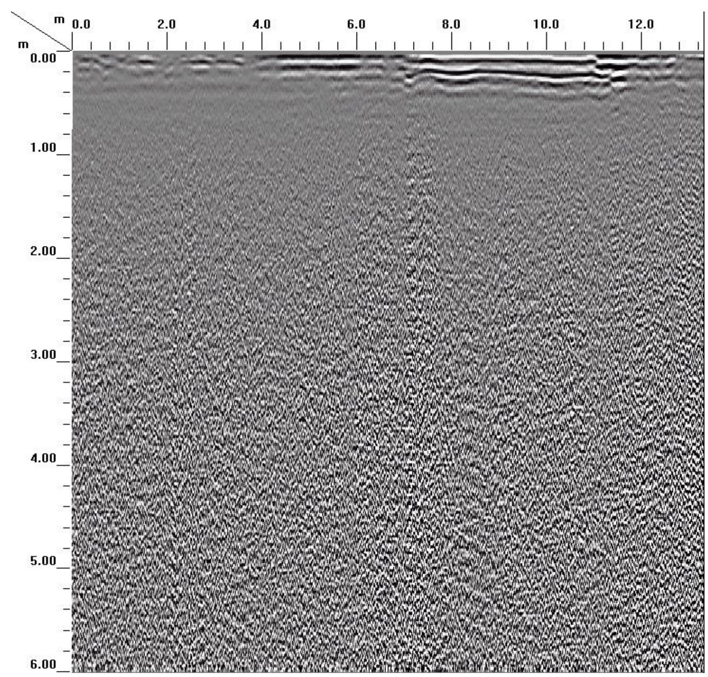
m
0.0
2.0
4.0
6.0
8.0
10.0
12.0
m
0.00
1.00
2.00
3.00
4.00
5.00
6.00

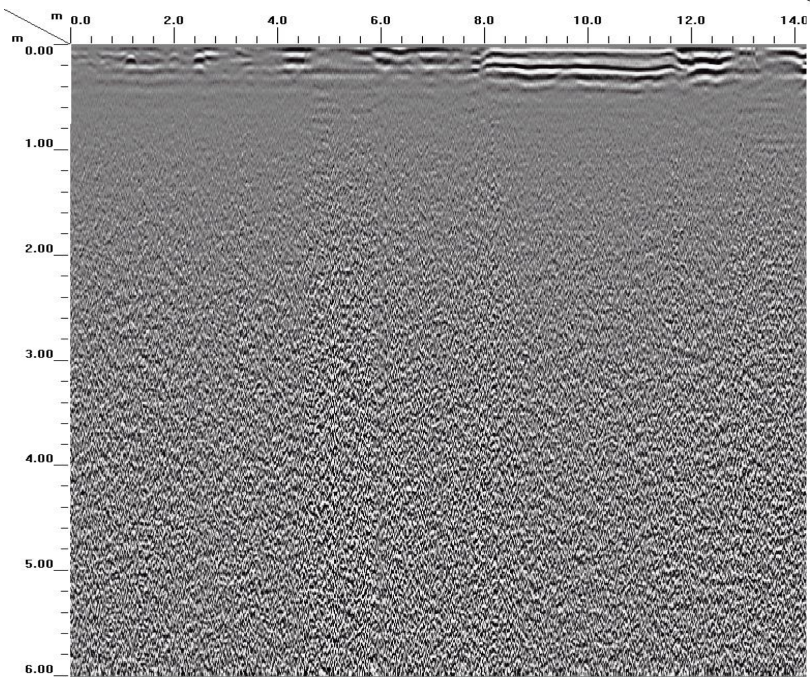
m
0.0
2.0
4.0
6.0
8.0
10.0
12.0
14.0
m
0.00
1.00
2.00
3.00
4.00
5.00
6.00

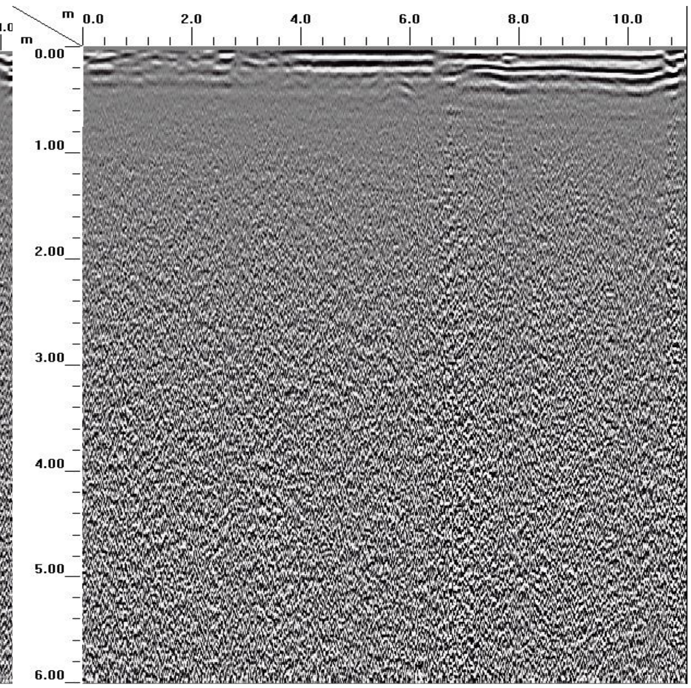
m
0.0
2.0
4.0
6.0
8.0
10.0
m
0.00
1.00
2.00
3.00
4.00
5.00
6.00

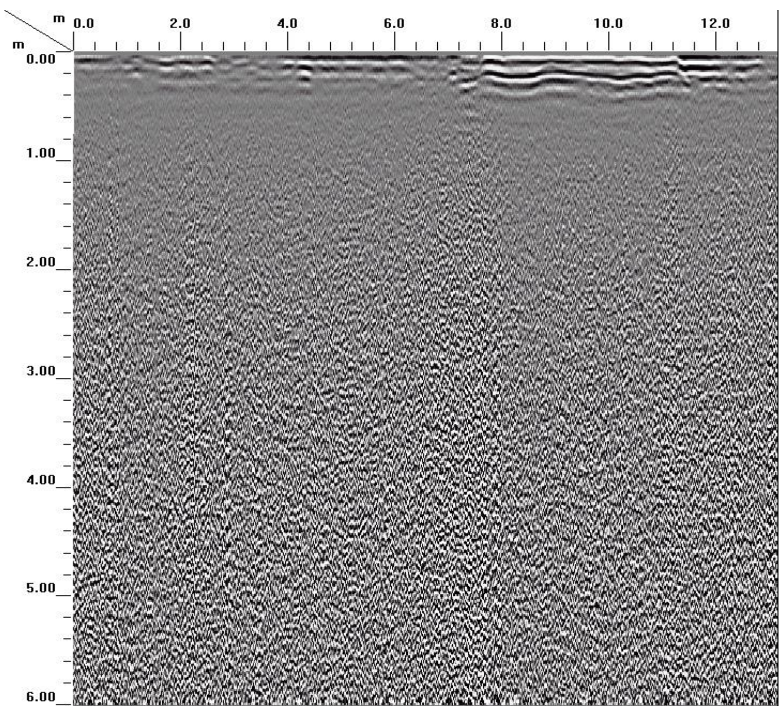
m
0.0
2.0
4.0
6.0
8.0
10.0
12.0
m
0.00
1.00
2.00
3.00
4.00
5.00
6.00

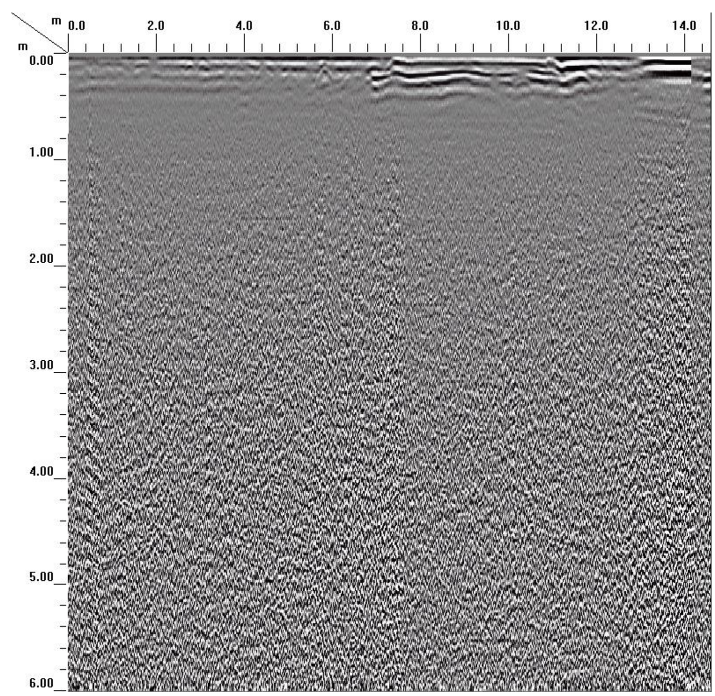
m
0.0
2.0
4.0
6.0
8.0
10.0
12.0
14.0
m
0.00
1.00
2.00
3.00
4.00
5.00
6.00

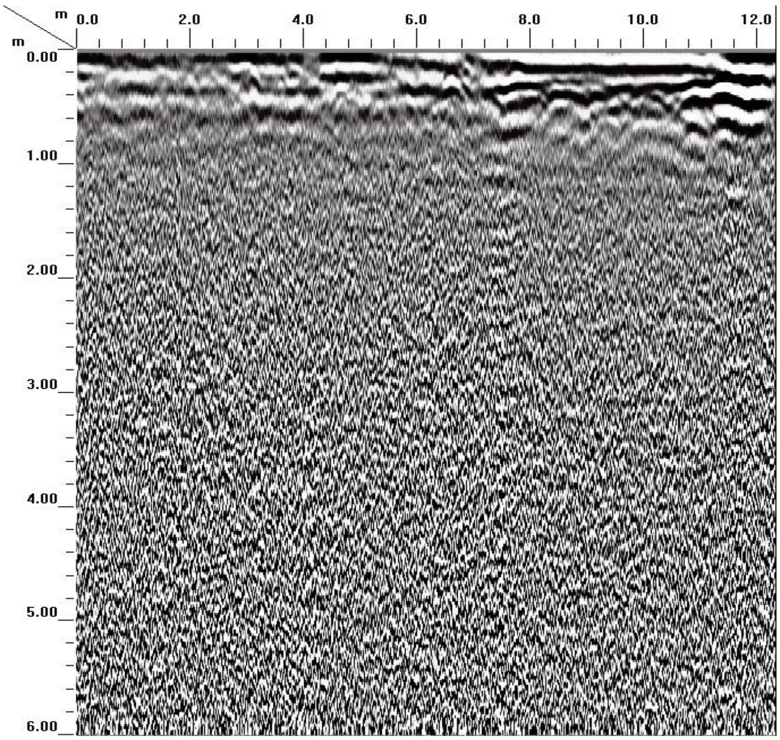
m
m
0.0
2.0
4.0
6.0
8.0
10.0
12.0
0.00
1.00
2.00
3.00
4.00
5.00
6.00

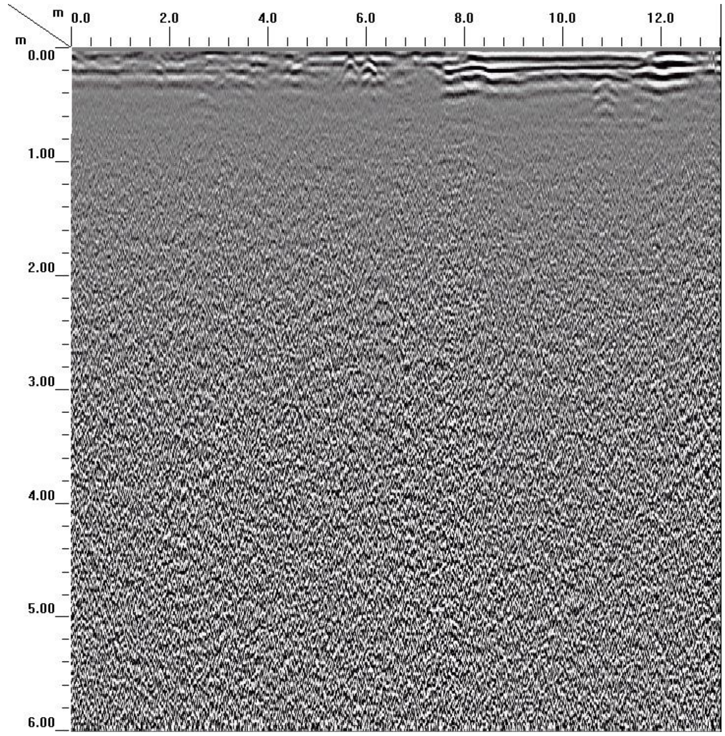
m
m
0.0
2.0
4.0
6.0
8.0
10.0
12.0
0.00
1.00
2.00
3.00
4.00
5.00
6.00

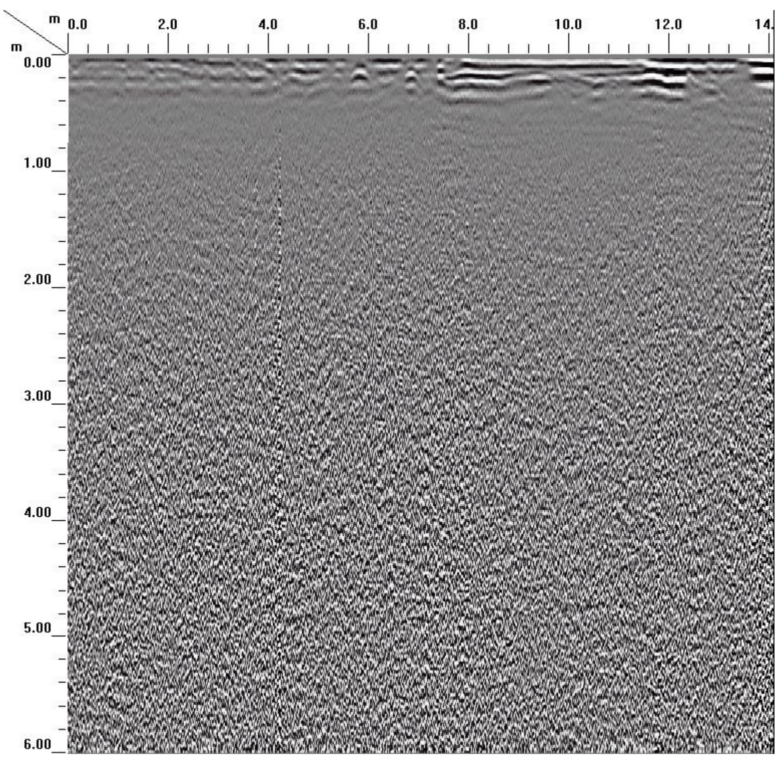
m
m
0.0
2.0
4.0
6.0
8.0
10.0
12.0
14
0.00
1.00
2.00
3.00
4.00
5.00
6.00

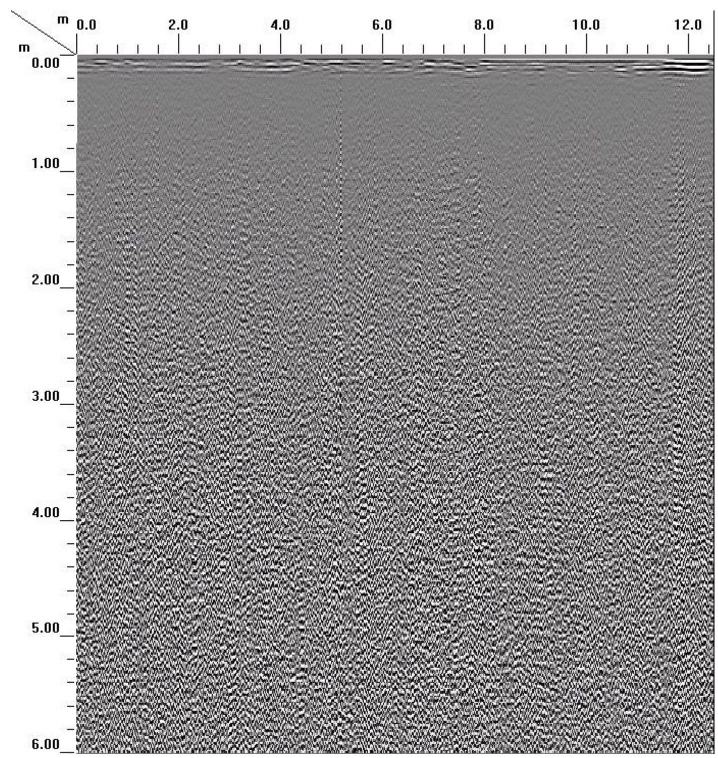
m
m
0.0
2.0
4.0
6.0
8.0
10.0
12.0
0.00
1.00
2.00
3.00
4.00
5.00
6.00

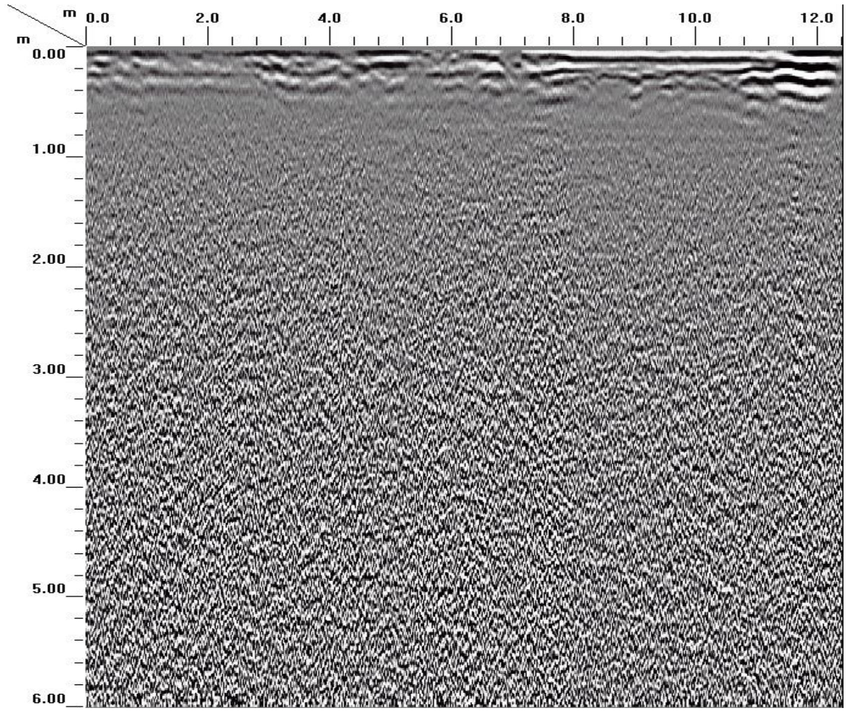

Figure B2: GPR Profile for GRID B (line 1 – 15).

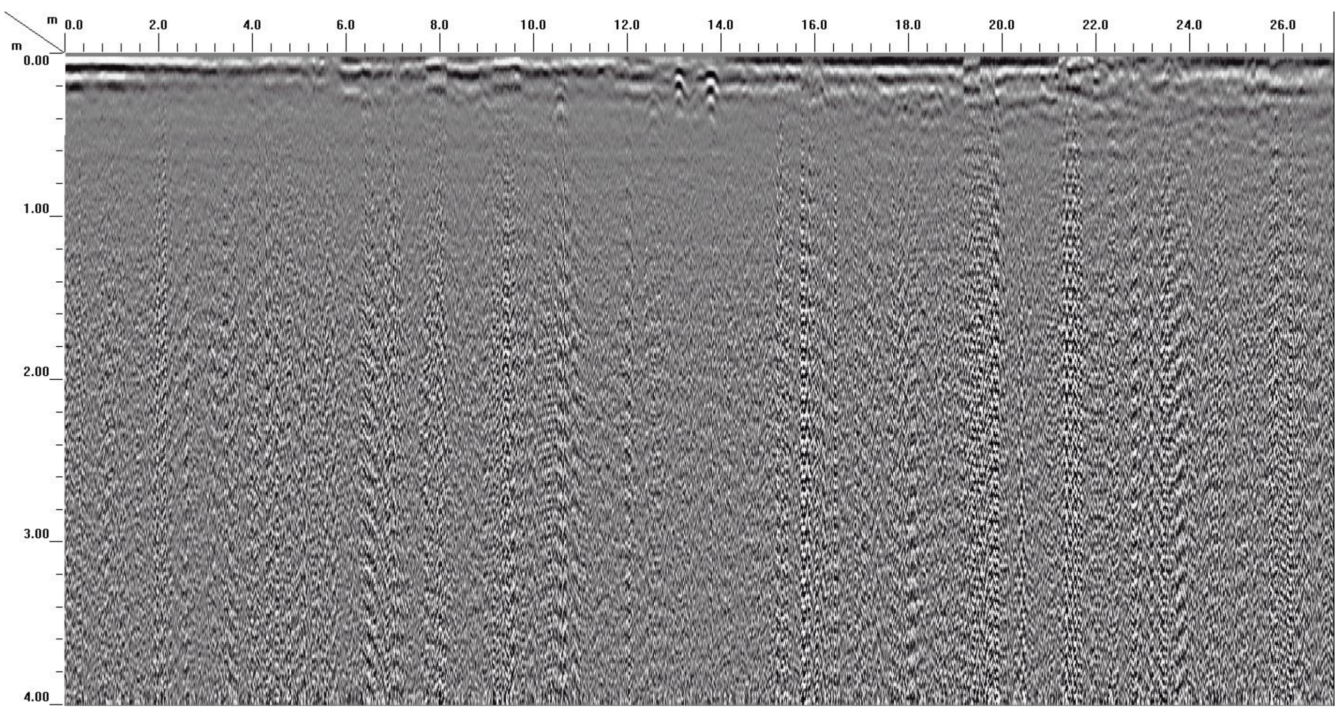

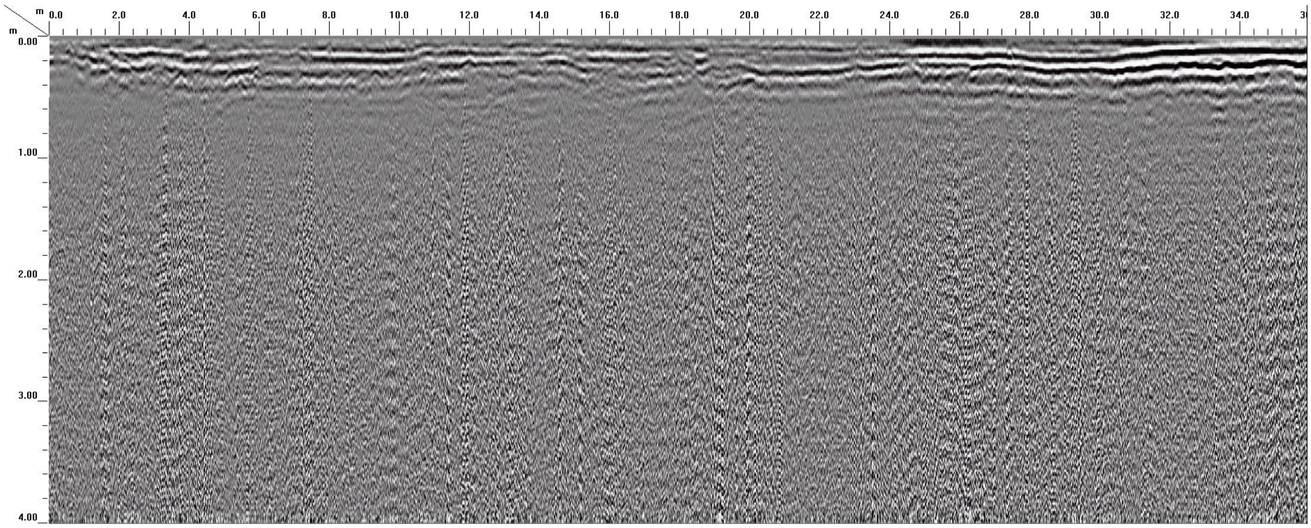
m
m
0.0
2.0
4.0
6.0
8.0
10.0
12.0
14.0
16.0
18.0
20.0
22.0
24.0
26.0
28.0
30.0
32.0
34.0
0.00
1.00
2.00
3.00
4.00

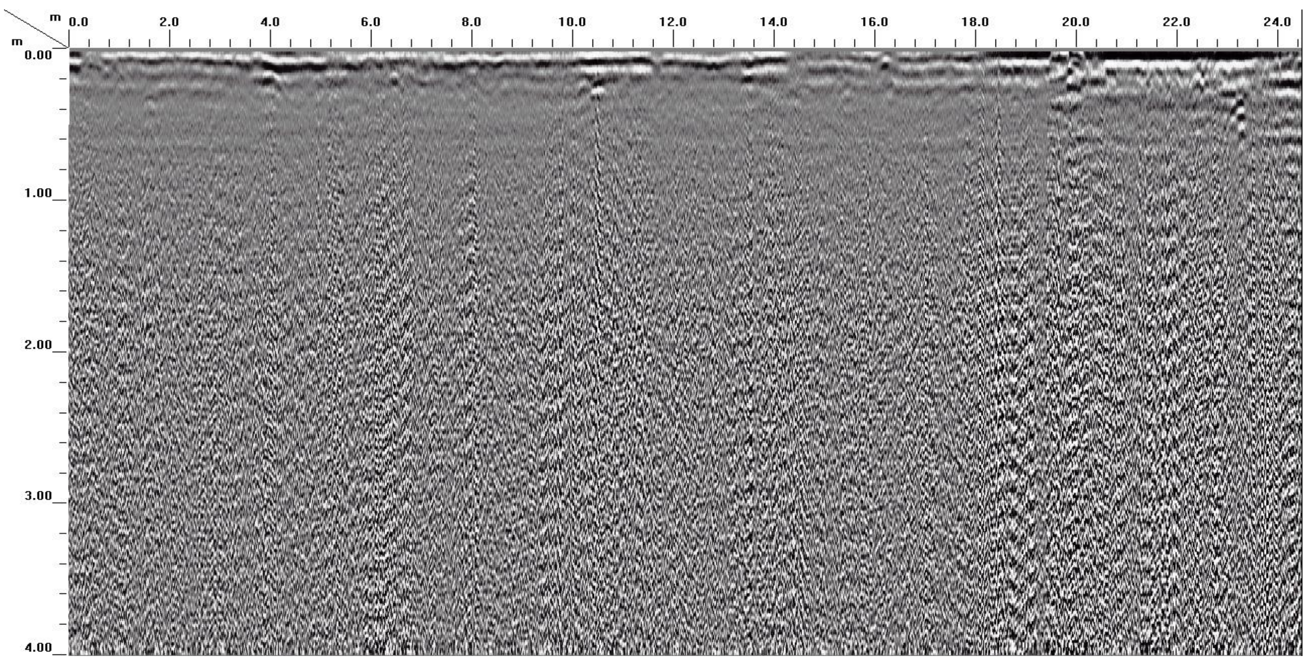
m
m
0.0
2.0
4.0
6.0
8.0
10.0
12.0
14.0
16.0
18.0
20.0
22.0
24.0
0.00
1.00
2.00
3.00
4.00

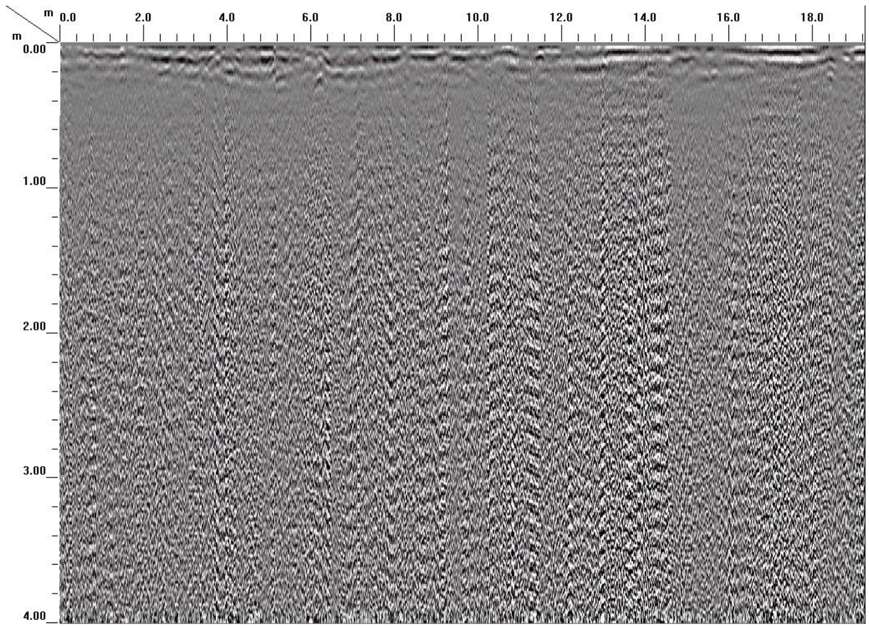

Figure B2: GPR profile for Grid C